CHAPMAN UNIVERSITY

Chapman University Digital Commons

Mathematics, Physics, and Computer Science Faculty Articles and Research

Science and Technology Faculty Articles and Research

2010

Climatological aspects of the optical properties of fine/coarse mode aerosol mixtures

Thomas F. Eck
Universities Space Research Association

B. N. Holben
NASA

Aliaksandyr Sinyuk
NASA

R. T. Pinker
University of Maryland - College Park

P. Goloub
Université de Lille, France

See next page for additional authors

Follow this and additional works at: https://digitalcommons.chapman.edu/scs_articles

 Part of the Atmospheric Sciences Commons, and the Environmental Monitoring Commons

Recommended Citation

Eck, T. F., et al. (2010), Climatological aspects of the optical properties of fine/coarse mode aerosol mixtures, *J. Geophys. Res.*, 115, D19205, doi:10.1029/2010JD014002.

This Article is brought to you for free and open access by the Science and Technology Faculty Articles and Research at Chapman University Digital Commons. It has been accepted for inclusion in Mathematics, Physics, and Computer Science Faculty Articles and Research by an authorized administrator of Chapman University Digital Commons. For more information, please contact laughtin@chapman.edu.

Climatological aspects of the optical properties of fine/coarse mode aerosol mixtures

Comments

This article was originally published in *Journal of Geophysical Research* , volume 115, in 2010. DOI: 10.1029/2010JD014002

Copyright

American Geophysical Union

Authors

Thomas F. Eck, B. N. Holben, Aliaksandyr Sinyuk, R. T. Pinker, P. Goloub, H. Chen, B. Chatenet, Z. Li, Ramesh P. Singh, Sachchida N. Tripathi, J. S. Reid, D. M. Giles, O. Dubovik, N. T. O'Neill, A. Smirnov, P. Wang, and X. Xia

This article is available at Chapman University Digital Commons: https://digitalcommons.chapman.edu/scs_articles/242

Climatological aspects of the optical properties of fine/coarse mode aerosol mixtures

T. F. Eck,[1,2] B. N. Holben,[1] A. Sinyuk,[1,3] R. T. Pinker,[4] P. Goloub,[5] H. Chen,[6] B. Chatenet,[7] Z. Li,[4] R. P. Singh,[8] S. N. Tripathi,[9] J. S. Reid,[10] D. M. Giles,[1,3] O. Dubovik,[5] N. T. O'Neill,[11] A. Smirnov,[1,3] P. Wang,[12] and X. Xia[12]

Received 3 February 2010; revised 19 May 2010; accepted 28 May 2010; published 1 October 2010.

[1] Aerosol mixtures composed of coarse mode desert dust combined with fine mode combustion generated aerosols (from fossil fuel and biomass burning sources) were investigated at three locations that are in and/or downwind of major global aerosol emission source regions. Multiyear monitoring data at Aerosol Robotic Network sites in Beijing (central eastern China), Kanpur (Indo-Gangetic Plain, northern India), and Ilorin (Nigeria, Sudanian zone of West Africa) were utilized to study the climatological characteristics of aerosol optical properties. Multiyear climatological averages of spectral single scattering albedo (SSA) versus fine mode fraction (FMF) of aerosol optical depth at 675 nm at all three sites exhibited relatively linear trends up to ~50% FMF. This suggests the possibility that external linear mixing of both fine and coarse mode components (weighted by FMF) dominates the SSA variation, where the SSA of each component remains relatively constant for this range of FMF only. However, it is likely that a combination of other factors is also involved in determining the dynamics of SSA as a function of FMF, such as fine mode particles adhering to coarse mode dust. The spectral variation of the climatological averaged aerosol absorption optical depth (AAOD) was nearly linear in logarithmic coordinates over the wavelength range of 440–870 nm for both the Kanpur and Ilorin sites. However, at two sites in China (Beijing and Xianghe), a distinct nonlinearity in spectral AAOD in logarithmic space was observed, suggesting the possibility of anomalously strong absorption in coarse mode aerosols increasing the 870 nm AAOD.

Citation: Eck, T. F., et al. (2010), Climatological aspects of the optical properties of fine/coarse mode aerosol mixtures, *J. Geophys. Res.*, *115*, D19205, doi:10.1029/2010JD014002.

1. Introduction

[2] Aerosol optical properties are difficult to characterize globally due to their large spatial and temporal variability. This results from the relatively short residence times in the atmosphere (days to weeks) and the large variability in composition and particle size resulting from a wide range of sources, both natural (primarily sea salt and desert dust) and anthropogenic (primarily combustion of biomass and fossil fuels). Mixtures composed of natural aerosols, which are predominately coarse mode particles (typically radius > ~1 μm), and combustion-produced particles that are predominately fine mode particles (typically radius < ~1 μm) of various mixed relative fractions are some of the most challenging types to characterize.

[3] Mixtures of desert dust aerosol with combustion-produced particles occur seasonally in some of the most active regions of aerosol emission in the world. For example, the Sahelian and Sudanian zones of northern Africa experience very high loadings of desert dust from sources in the Sahara and Sahel for most of the year. However, these dust particles mix with biomass burning aerosols from numerous

[1]Biospheric Sciences Branch, NASA Goddard Space Flight Center, Greenbelt, Maryland, USA.
[2]Goddard Earth Sciences and Technology Center, University of Maryland, Baltimore, Maryland, USA.
[3]Sigma Space Corporation, Lanham, Maryland, USA.
[4]Department of Atmospheric and Oceanic Science, University of Maryland, College Park, Maryland, USA.
[5]Laboratoire d'Optique Atmospherique, Université de Lille 1, Villeneuve d'Ascq, France.
[6]Division for Middle Atmosphere and Remote Sensing, Chinese Academy of Sciences, Beijing, China.
[7]LISA, Universités Paris-Est - Paris Diderot-Paris 7, CNRS, Créteil, France.
[8]Computational Science and Engineering, Chapman University, Orange, California, USA.
[9]Department of Civil Engineering, Indian Institute of Technology Kanpur, Kanpur, India.
[10]Marine Meteorology Division, Naval Research Laboratory, Monterey, California, USA.
[11]CARTEL, Universite de Sherbrooke, Sherbrooke, Quebec, Canada.
[12]LAGEO, Institute of Atmospheric Physics, Chinese Academy of Sciences, Beijing, China.

Copyright 2010 by the American Geophysical Union.
0148-0227/10/2010JD014002

fires occurring in the Sahel and Sudanian zones primarily during the months of November through March [*Cooke et al.*, 1996; *Dwyer et al.*, 2000] in various relative concentrations. Some other regions have seasonal mixtures of desert dust with fine mode aerosols produced mainly from fossil fuel combustion (although biomass burning also contributes). Two regions with very high aerosol concentrations and typically mixed fine-coarse aerosols in spring (primarily March–June) due to dust storms are northern India and northeastern China. Mixed fine and coarse aerosols from all of these regions affect large continental regions but are also seasonally advected over significant areas of ocean as well. Of course aerosol mixtures also occur in many other regions, but typically in lower concentrations than occur in these three regions. It is noted that sometimes the aerosols are well mixed within a single layer or layers while at other times aerosol layers of different particle types occur at differing altitudes [*Schmid et al.*, 2003; *Redemann et al.*, 2003; *Johnson et al.*, 2008].

[4] Knowledge of the variability in absorption of these aerosol mixtures is particularly important for assessing the direct forcing of these aerosol types and the semidirect forcing that may occur from atmospheric heating by absorbing aerosol layers. Mixtures of desert dust and combustion aerosols contain the two primary particulate absorbing species, black carbon in fine mode particles [*Bond and Bergstrom*, 2006] and iron oxides in coarse mode dust [*Sokolik and Toon*, 1999]. In desert dust aerosols, iron oxides cause the strongest absorption in the ultraviolet through the visible wavelengths [*Derimian et al.*, 2008a]. In combustion-produced aerosols the principal absorber is soot or black carbon, which exhibits absorption throughout the entire solar spectrum due to a relatively spectrally constant imaginary index of refraction [*Bergstrom et al.*, 2002].

[5] Accurate knowledge of the magnitude of aerosol absorption is important in quantitative evaluation of the potential aerosol influence on the Indian monsoon circulation. Several recent studies [*Lau et al.*, 2006; *Ramanathan et al.*, 2005; *Meehl et al.*, 2008] have suggested that absorbing aerosols may be shifting the timing and intensity of the Indian monsoon circulation. The modeling study of *Menon et al.* [2002] suggests that absorbing aerosols in China may be responsible in part for circulation changes that may result in a drying trend in northern China and a simultaneous shift to higher rainfall amounts in southern China, although the value of the single scattering albedo assumed in their modeling (0.85) appears to be systematically lower than those inferred from measurements made across China (mean ~ 0.9) [*Zhao and Li*, 2007; *Lee et al.*, 2007]. In West Africa, *Huang et al.* [2009] analyzed satellite data and concluded that aerosol affects the large-scale variability in precipitation associated with the West African monsoon. Additionally *Mallet et al.* [2009] simulated significant reductions in convective activity associated with absorbing dust in West Africa. In the current study, we focus on mixtures of coarse mode dominated desert dust with fine mode combustion aerosols utilizing aerosol robotic network (AERONET) data acquired at three sites: Beijing (China), Kanpur (India), and Ilorin (Nigeria). These long-term AERONET monitoring sites with several years of data were chosen to provide information on aerosol optical properties that may be analyzed in a climatological sense given that the average dynamics of these mixtures can be investigated due to sufficiently large data samples. Also the high aerosol optical depths measured at all of these sites allow for robust analyses of aerosol absorption since sensitivity to absorption in AERONET retrievals increases as aerosol optical depth (AOD) increases [*Dubovik et al.*, 2000]. The dynamics of aerosol absorption, as parameterized by the single scattering albedo (SSA or ω_0), of these mixtures are a particular focus of this paper since SSA is the most important aerosol parameter that remains relatively poorly quantified.

2. Instrumentation, Study Sites, and Techniques

2.1. Study Regions and Sites

[6] The study focused on AERONET sites that are all located in and/or downwind of some of the major aerosol source regions on Earth. The principal sites analyzed in this paper (Figure 1) had multiyear measurement databases that range from 5 to 8 years of data for every month. The aerosol optical depths measured at these sites had some of the highest annual means of all sites monitored over the history of AERONET. Beijing, China is a megacity of population ~17 million in 2009, with many additional high-density population centers in the region of eastern China. Heavy pollution aerosol was present in all months, mainly from fossil fuel combustion, and desert dust events that occur primarily in the spring season (March–May) [*Eck et al.*, 2005]. This desert dust is advected from the Taklamakan desert in western China, from less distant Chinese desert regions west of Beijing, and also from Mongolia. The Kanpur site in India is located immediately to the northwest of Kanpur, an industrial city with population ~5 million in 2009. The Indo-Gangetic Plain region where Kanpur is located is a major emission source of pollution aerosol from the combustion of fossil fuels and biofuels [*Singh et al.*, 2004; *Novakov et al.*, 2000; *Venkataraman et al.*, 2005; *Prasad et al.*, 2006]. Also in spring and early summer, the aerosol type dynamics at Kanpur was strongly influenced by desert dust advected eastward from the Thar desert of the India/Pakistan border region and from arid regions farther west in the Middle East. Ilorin, Nigeria is a city of population ~1 million and is located downwind of one of the single largest dust sources on Earth, the Bodele depression in Chad [*Todd et al.*, 2007; *Prospero et al.*, 2002]. Additionally, extensive biomass burning occurs throughout the region and in the Sahel to the north, primarily during November through March.

2.2. AERONET Instrumentation

[7] The CIMEL Electronique CE-318 Sun-sky radiometer measurements were made with instruments that are a part of the AERONET global network. These instruments are described in detail by *Holben et al.* [1998]; however, a brief description is given here. The automatic tracking Sun and sky scanning radiometers made direct Sun measurements with a 1.2° full field of view every 15 min at 340, 380, 440, 500, 675, 870, 940, and 1020 nm (nominal wavelengths). However, for the Beijing site the version of the CIMEL installed there most years had only the 440, 675, 870, and 1020 nm channels for AOD measurement. The direct Sun measurements take ~8 s to scan all eight wavelengths (repeated 3 times within a minute), with a motor-driven

Figure 1. Map showing the three principal AERONET sites analyzed, Ilorin (Nigeria), Kanpur (India), and Beijing (China).

filter wheel positioning each filter in front of the detector. These solar extinction measurements are used to compute aerosol optical depth (AOD or τ_a) at each wavelength except for the 940 nm channel, which is used to retrieve total column (or precipitable) water vapor in centimeters. The filters utilized in these instruments were ion assisted deposition interference filters with band pass (full width at half maximum) of 10 nm, except for the 340 and 380 nm channels at 2 nm. The estimated uncertainty in computed τ_a, due primarily to calibration uncertainty, is ~0.010–0.021 for field instruments (which is spectrally dependent with the higher errors in the UV) [*Eck et al.*, 1999]. *Schmid et al.* [1999] compared τ_a values derived from four different solar radiometers (including an AERONET Sun-sky radiometer) operating simultaneously together in a field experiment and found that the τ_a values from 380 to 1020 nm agreed to within 0.015 (rms), which is similar to our estimated level of uncertainty in τ_a retrieval for field instruments. Only AERONET version 2 level 2 AOD data have been analyzed. The spectral aerosol optical depth data have been screened for clouds following the methodology of *Smirnov et al.* [2000], which relies on the higher temporal frequencies of cloud optical depth versus aerosol optical depth. The sky radiances measured by the Sun/sky radiometers are calibrated versus frequently characterized integrating spheres at the NASA Goddard Space Flight Center to an absolute accuracy of ~5% or better [*Holben et al.*, 1998].

2.3. Inversion Methodology

[8] The CIMEL sky radiance measurements in the almucantar geometry (fixed elevation angle equal to solar elevation and a full 360° azimuthal sweep) at 440, 675, 870, and 1020 nm (nominal wavelengths) in conjunction with the direct Sun measured τ_a at these same wavelengths were used to retrieve optical equivalent, column-integrated aerosol size distributions and refractive indices. Using this microphysical information the spectral dependence of single scattering albedo is calculated. The algorithm of *Dubovik and King* [2000] with enhancements detailed in the work of *Dubovik et al.* [2006] was utilized in these retrievals, known as version 2 AERONET retrievals. Only version 2 and level 2 quality-assured retrievals [*Holben et al.*, 2006] are presented in this paper. The version 2 AERONET algorithm determines the percentage of spherical and spheroidal particles required to give the best fit to the measured spectral sky radiance angular distribution. Further details on the version 2 algorithm and the improved specification of surface bidirectional reflectance can be found in the works of *Dubovik et al.* [2006] and *Eck et al.* [2008].

[9] Almucantar sky radiance measurements were made at optical air masses of 4, 3, 2, and 1.7 in the morning and afternoon and once per hour in between. In order to ensure sky radiance data over a wide range of scattering angles, only almucantar scans at solar zenith angles greater than 50° are analyzed and presented here. To eliminate cloud contamination from the almucantar directional sky radiance data AERONET requires the radiances to be symmetrical on both sides of the Sun at equal scattering angles, and symmetric radiances from both sides are subsequently averaged. The stable performance of the inversion algorithm was illustrated in sensitivity studies performed by *Dubovik et al.* [2000] where the perturbations of the inversion resulting from random errors, possible instrument offsets, and known uncertainties in the atmospheric radiation model were analyzed. Their work employed retrieval tests using known size distributions to demonstrate successful retrievals of mode radii and the relative magnitude of modes for various types of bimodal size distributions such as those dominated by a submicron accumulation mode or distributions dominated by supermicron coarse mode aerosols. To ensure sufficient

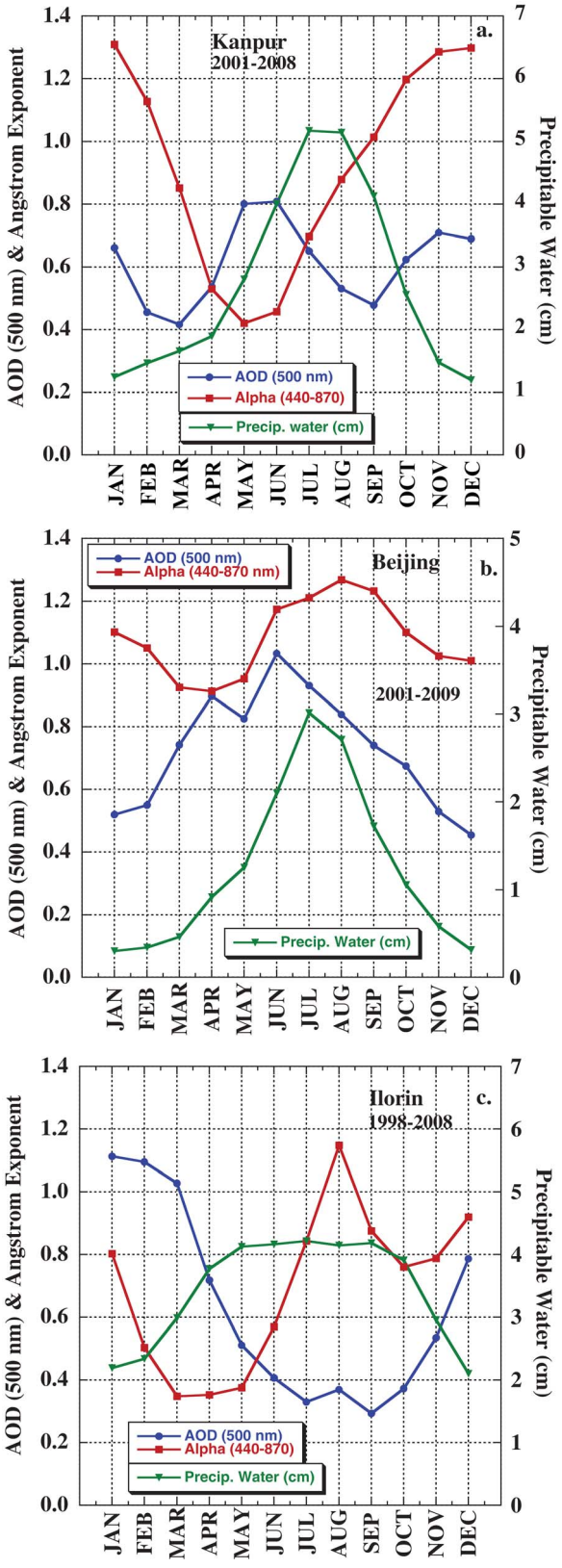

Figure 2. Monthly means of AOD (500 nm), Angstrom exponent (440–870 nm), and precipitable water computed from multiyear monitoring at AERONET sites located in (a) Kanpur, India; (b) Beijing, China; and (c) Ilorin, Nigeria.

sensitivity to aerosol absorption, only almucantar scans where AOD(440 nm) > 0.4 [*Dubovik et al.*, 2000] were analyzed for the investigation of the characteristics of spectral refractive indices and single scattering albedo. For fine mode biomass burning aerosols in southern Africa *Leahy et al.* [2007] found a mean discrepancy in 550 nm SSA between in situ measurements and AERONET retrievals of −0.01 for five coincident flights over AERONET sites. Discussion of comparisons between AERONET retrievals and in situ measurements of SSA for fine and coarse mode aerosol mixtures are given below in section 3.3.3.

3. Results and Discussion

3.1. Multiyear Climatology of AOD and Angstrom Exponent

[10] In this section, we present the monthly mean AOD, Angstrom exponent (440–870 nm), and total column precipitable water for each of the three AERONET sites studied. The 440–870 nm Angstrom exponent ($\alpha_{440-870}$) is computed from linear regression of ln AOD versus lnλ for all AOD data available between the wavelengths of 440 and 870 nm. Monthly means of all parameters are computed using data available for each site, from 5 to 8 years for each given month. This length of data record enables a reasonable characterization of the annual seasonal cycle due to variations in meteorological conditions and aerosol source strengths.

[11] At Kanpur, India (Figure 2a), a pronounced seasonal cycle is exhibited by the Angstrom Exponent with maximum values in the late fall and winter months (October–February) when $\alpha_{440-870}$ exceeds 1.1, and minimum values in the premonsoon months of April–June (less than 0.55). This very large seasonality in $\alpha_{440-870}$ is the result of dominance by fine mode pollution aerosols in the winter and dominance by coarse mode desert dust aerosols in the premonsoon months, due to seasonal variations in soil moisture and winds that result from the monsoon circulation cycle. The fine mode aerosols in the Indo-Gangetic Plain of northeastern Pakistan and India are produced by a combination of combustion sources including coal fired power plants, vehicle emissions, numerous industries, and domestic biomass burning of fuel wood and dung. The fine mode aerosol emission rate does not vary strongly over the annual cycle; however, the dust emissions that are advected toward Kanpur do have a pronounced seasonality. It is noted however that some variation in fine mode emissions occur, with more biomass burning fires in the premonsoon season and more domestic fuel consumption for heating in the winter. The strong cycle in total column water vapor, with values exceeding 4 cm from June to September, is associated with the seasonality in monsoon precipitation, with ~88% of the annual rainfall total of ~1020 mm occurring during the monsoon months of June–September. The seasonal cycle in AOD shows a maximum in May and June (minimum $\alpha_{440-870}$ occurs then also) coinciding with a peak in dust generation activity. A secondary maximum occurs from November through January; however, the aerosol loading is high all year, with all months having average 500 nm AOD > 0.4.

[12] The annual cycle of monthly mean Angstrom Exponent at Beijing, China, shows a much lower range as compared to Kanpur, with all but 3 months having values between ~1.0 and ~1.3, therefore clearly dominated by fine mode

aerosol for most of the year (Figure 2b). The spring months of March, April, and May are the dust season months [*Huebert et al.*, 2003] with maximum advection of desert dust from arid regions of western China and Mongolia toward eastern China. However, even during these months the average Angstrom exponent ranged from 0.91 to 0.95; thus, in the spring the fine mode pollution AOD still exceeds the coarse mode AOD in the midvisible wavelengths [*Eck et al.*, 2005]. Monthly mean 500 nm AOD values reach a maximum in June (~1.03) and exceed 0.7 from March through September, and the minimum values occur during the late fall and winter months of November through February, when monthly mean AOD range from ~0.45 to ~0.55, still very high values. The monthly mean column water vapor exceeds ~1.7 cm from June through September, during which ~83% of the annual total precipitation of ~640 mm occurs.

[13] The primary sources of aerosol in Ilorin, Nigeria are desert dust from the Sahara and the Sahel region advected from the north and biomass burning of primarily savanna in the Sahel and Sudanian zones during the burning season of November through March. The aerosol regime of this site is more strongly influenced by desert dust than the other two sites, with monthly mean $\alpha_{440-870} \sim 0.8$ or less during 8 months of the year (Figure 2c). The peak dust dominated months are February through June when average $\alpha_{440-870} < 0.6$, while the highest monthly mean $\alpha_{440-870}$ occurs in August at 1.15. Monthly mean 500 nm AOD has a wide annual range at this site from a high of ~1.10 in both January and February when combined desert dust and biomass burning emissions are strong [*Haywood et al.*, 2008; *Johnson et al.*, 2008] to an annual low monthly mean of 0.29 in September. Rainfall is relatively high during the 7 months from April through October (~92% of annual rainfall; column water vapor exceeds ~3.8 cm for all of these months) with monthly totals exceeding 100 mm for each of these months. The relatively low monthly mean AOD during these months suggests that aerosol washout, and circulation changes associated with the high rainfall result in lowered aerosol loadings.

3.2. Relationships Between Angstrom Exponent and Fine Mode Fraction of AOD

[14] The Angstrom exponent is often used to give an indication of the relative magnitude of the fine and coarse mode contributions to the total extinction AOD [*Eck et al.*, 1999; *Holben et al.*, 2001]. In this section, we examine the relationship between the Angstrom exponent and the fine mode fraction (FMF) of the AOD that are determined using two independent methodologies from the AERONET data and retrievals.

[15] First, we examine the fine mode fraction of AOD that has been computed based on the retrieved size distributions and spectral refractive indices from the *Dubovik and King* [2000] algorithm applied to AERONET almucantar scans, assuming bimodal size distributions. The maximum radius of the fine mode volume distribution was defined as the minimum (or inflection point) between the fine and coarse modes in the retrieved size distribution, over the defined range limits of 0.44–0.99 μm radius. The minimum radius for the fine mode is fixed at 0.05 μm radius, which is the minimum radius of the almucantar inversion. The relationship between this fine mode fraction of optical depth and $\alpha_{440-870}$ for 5 years of observations at Kanpur, India is shown in Figure 3a. Fine mode fraction of AOD at a fixed $\alpha_{440-870}$ value (especially < 1.1) decreases strongly as wavelength increases since fine mode particles (peak radius ranging from ~0.11 to ~0.30 μm) scatter light most effectively at wavelengths similar to particle size, but are much less effective light scatters when the wavelength is significantly longer than particle size. The relationship between FMF and $\alpha_{440-870}$ is much more linear in the visible than the near infrared wavelengths, suggesting much greater sensitivity to fine/coarse mixtures in the visible. As Angstrom exponent increases, especially >1.1, there is much greater scatter in the fine mode fraction for a given $\alpha_{440-870}$ value, at all wavelengths. This is largely the result of differences in fine mode particle size and the reduction in α magnitude as fine mode particles grow from aging and/or hygroscopic growth [*Reid et al.*, 1999; *Eck et al.*, 2001, 2003].

[16] Comparison of the FMF of AOD at 500 nm versus $\alpha_{440-870}$ between the *Dubovik and King* [2000] retrieval (interpolated from the 440 and 675 nm data) to the spectral deconvolution algorithm (SDA) methodology [*O'Neill et al.*, 2001, 2003] for Kanpur is shown in Figure 3b (both level 2). The SDA algorithm utilizes only the spectral AOD observations from 380 to 870 nm (five wavelengths) as input, while the Dubovik algorithm utilizes the spectral AOD and angular sky radiance distributions at four wavelengths (440, 675, 870, and 1020 nm). Note that there was a factor of ~1.7 more days when the SDA inferred FMF than from the almucantar retrievals. The increased number of SDA retrievals occurs since spectral AOD measurements are made throughout the day when the solar disc is not obscured by clouds, while the almucantar retrieval requires that most sky radiances be cloud free and homogeneous in addition to the Sun being unobscured and solar zenith angle greater than 50° for the most robust retrievals. The two algorithms compute very similar FMF of AOD at 500 nm despite significant differences between the two techniques, and both show a very linear relationship up to $\alpha_{440-870}$ of ~1.1. The Dubovik FMF of AOD at 500 nm is ~0.05 higher on average than SDA FMF, for $\alpha_{440-870}$ ranging from ~0 to ~1.1, possibly due to the small sized particle "wing" of the coarse mode attributed to coarse mode AOD in the SDA algorithm, while this wing is included in the fine mode of the Dubovik algorithm since a particle radius cutoff is selected to define the two modes [*O'Neill et al.*, 2003]. Another possible reason for the bias could be that the SDA retrieval does not explicitly account for effects of variation in the refractive index, which is a source of SDA retrieval error.

[17] The fine mode fraction of AOD (computed from the Dubovik algorithm) as a function of $\alpha_{440-870}$ for Beijing, China (from 2001 to 2007 data) is shown in Figure 3c. It is noted that the relationships are quite similar to those observed for Kanpur in Figure 3a, which suggests similarity in aerosol optical properties between the two sites. In fact, size distributions at both sites show similar strong tendencies for growth in fine mode volume radius as FMF increases (see sections 3.3.1 and 3.3.2 below), and spectral SSA is also quite similar over the entire range of FMF values (see Figure 9 in section 3.3.2). Somewhat larger scatter was found in FMF at higher Angstrom values for Beijing however, likely due to the greater dynamics of fine mode particle size there as compared to Kanpur (sections 3.3.1 and 3.3.2 below). For

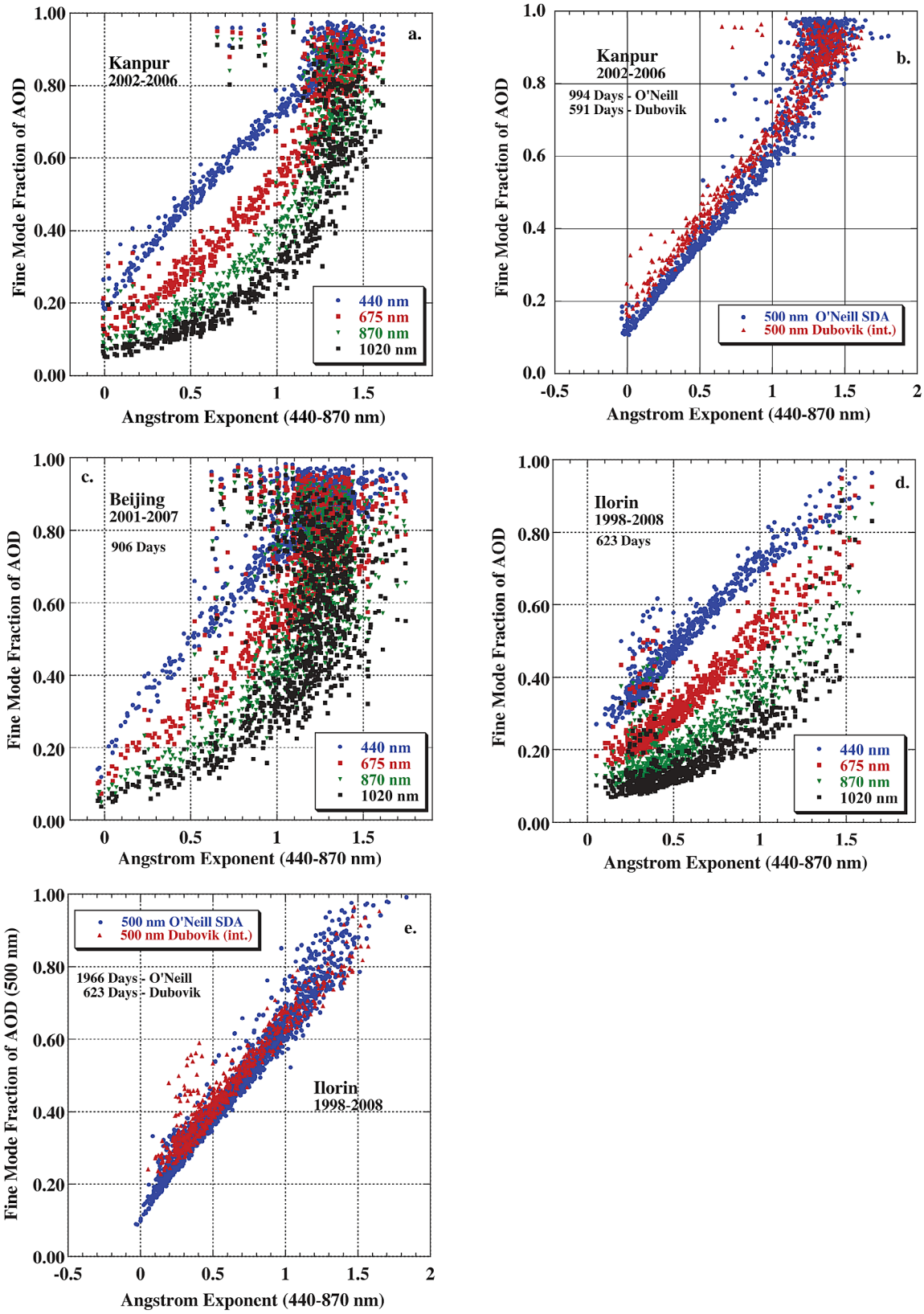

Figure 3. (a) Spectral fine mode fraction of AOD versus Angstrom Exponent (440–870 nm) at Kanpur, with FMF computed from the Dubovik algorithm almucantar retrievals. (b) The fine mode fraction of AOD at 500 nm, computed from both the O'Neill spectral deconvolution algorithm and the Dubovik almucantar retrievals, as a function of the Angstrom exponent (440–870 nm). (c) Similar to Figure 3a, but for Beijing. (d) Similar to Figure 3a, but for Ilorin. (e) Similar to Figure 3b, but for Ilorin.

example, *Eck et al.* [2003] have shown that the 440–870 nm Angstrom exponent for fine mode dominated smoke from different sources varied from ~1.1 to 2.0 due to differences in fine mode radius. The SDA values of FMF were not computed since the CIMEL instrument type used in Beijing (for most years) lacked the 380 and 500 nm channels, which are important channels needed to obtain the highest accuracy retrievals from this algorithm.

[18] The spectral FMF versus $\alpha_{440-870}$ for Ilorin, Nigeria (Figure 3d) differs from that of both Kanpur and Beijing at larger $\alpha_{440-870}$. Although the linear relationships for all sites are similar for $\alpha_{440-870} < 1.1$, there is a lack of variability and scatter at Ilorin for the large Angstrom values. This can be explained by the nearly constant value of fine mode particle radius over the entire range of Angstrom exponent at Ilorin (see Figure 12b in section 3.3.3). This lack of fine mode particle dynamic is likely due to a combination of factors, including the fact that typically fine mode biomass burning particles are only weakly hygroscopic as compared to the fossil fuel combustion aerosols that include much more sulfate which is strongly hygroscopic [*Kotchenruther and Hobbs*, 1998]. Additionally, the fine mode AOD values are often much higher at both Beijing and Kanpur resulting in higher rates of fine particle coagulation growth due to higher aerosol concentrations. At Ilorin the Dubovik FMF of AOD at 500 nm is ~0.03 higher than the SDA FMF (Figure 3e), for $\alpha_{440-870}$ ranging from ~0 to ~1, likely due to the same reasons mentioned for Kanpur (see Figure 3b). There was a factor of ~3 more days when the SDA retrieved the FMF as compared to the almucantar retrievals at Ilorin (for similar reasons as described for Figure 3b at Kanpur). Additionally, there are many SDA retrievals made at lower Angstrom exponent (minimum of about −0.05) than from the almucantar retrievals (minimum of ~0.1), possibly since these cases with only the largest particles present may be less homogeneous in sky radiances, which could occur during dust/sand storms.

3.3. Climatologies of Retrieved Single Scattering Albedo and Size Distributions

3.3.1. Kanpur, India

[19] Five years of almucantar scan retrievals (2002–2006) acquired at Kanpur were utilized to compute mean spectral single scattering albedos and size distributions for AOD (440) > 0.4 (Figures 4a and 4b). These values were averaged for the 675 nm fine mode fraction (FMF) of AOD bins with ranges of 0–0.2, 0.2–0.3, 0.3–0.4, …, 0.8–0.9, 0.9–1.0 (nine bins). The first bin is larger since the minimum 675 nm FMF observed for an individual almucantar scan was 0.09. Coarse mode dominated observations (<50% FMF) comprise 40% of the total retrievals while fine mode dominated cases were 60% of the total, with averages computed from over 100 almucantar retrievals per bin. The most frequently occurring FMF was 0.8–0.9 with 25% of the total observations. The wavelength of 675 nm was chosen for FMF from the four almucantar measurement wavelengths since it is approximately at the center of the downwelling solar irradiance spectrum, with ~50% of the spectrally integrated flux falling above or below this wavelength. The single scattering albedo as a function of FMF (Figure 4a) shows very little variation at 440 nm, yet a large dynamic range at the three longer wavelengths (675, 870, and 1020 nm). At 440 nm the range in SSA is restricted to values of 0.87–0.89 for all but the highest FMF bin, therefore suggesting both coarse mode aerosol dominated mixtures (desert dust) and fine mode dominated aerosol mixtures (pollution) have similar relative magnitudes of absorption relative to scattering at this wavelength. Dust absorption is strongest in the UV and short wavelength visible and weak in the near infrared [*Sokolik and Toon*, 1999], while the main absorber in fine mode aerosol is black carbon, which exhibits strong absorption throughout this wavelength interval due to a relatively spectrally constant value of the imaginary refractive index [*Bergstrom et al.*, 2002]. The higher SSA at 440 nm for the 0.93 FMF bin is largely due to the larger fine mode particle size causing greater scattering, with increasing radius as FMF increases (Figure 4b). This increase in fine mode particle size likely occurs mainly due to increased coagulation rates as fine mode AOD (and concentrations) increase [*Colarco et al.*, 2004]. The imaginary part of the refractive index (k) at 440 nm varies from 0.013 to 0.018 for all bins with FMF >50% and with no monotonic trend as a function of FMF. The k value is ~0.015 for the 0.93 FMF average interval, therefore suggesting a similar amount of black carbon as the other fine mode dominated bins, but with larger particle radius. The relatively small dynamic range of SSA at 440 nm compared to other wavelengths suggests a significant advantage at 440 nm in the satellite retrieval of AOD in the Indo-Gangetic Plain (i.e., deep blue algorithm) [*Hsu et al.*, 2004], since most satellite retrieval algorithms must assume the magnitude of aerosol absorption. Currently few retrieval algorithms have the means to dynamically select variable SSA or have sufficient sensitivity to aerosol absorption [*Remer et al.*, 2005; *Martonchik et al.*, 1998; *Kahn et al.*, 2005)]. The average volume median radius of the coarse mode varied from 2.34 μm at FMF of 0.16 to 2.88 μm at FMF of 0.93. A possible reason for larger observed radius at higher FMF may be coarse mode fly ash and other sources during high FMF pollution dominated events versus slightly smaller coarse mode dust particles during desert dust-dominated events. This relatively small range of coarse mode particle size does not result in significant differences in coarse mode absorption.

[20] Similar analysis of the SSA and size distributions as a function of 675 nm FMF of AOD for the premonsoon months of April, May, and June only are shown in Figures 4c and 4d. These 3 months have the lowest monthly mean Angstrom exponents at Kanpur, which range from approximately 0.45 to 0.55. Only 4% of the almucantar retrievals during these three months show a dominance of fine mode aerosol in the optical depth, with FMF at 675 nm > 0.50. Using a different methodology to compute component fractions of AOD at Kanpur, *Dey and Tripathi* [2008] found that premonsoon months 500 nm AOD fine fraction varied from ~0.50 to ~0.37 for April–June, higher than from our analysis (0.28 seasonal mean at 675 nm). However, the shorter wavelength of 500 nm for their analysis may explain a significant portion of the higher fine mode fraction at that wavelength (see Figure 3a). Although fine mode pollution aerosols are continually being produced by combustion of fossil and biomass fuels, dust aerosol has a dominant presence in the columnar AOD during this season. Both the SSA and size distributions are almost the same as in Figures 4a and 4b except for the averages at FMF of 0.54 and 0.66, which had too few

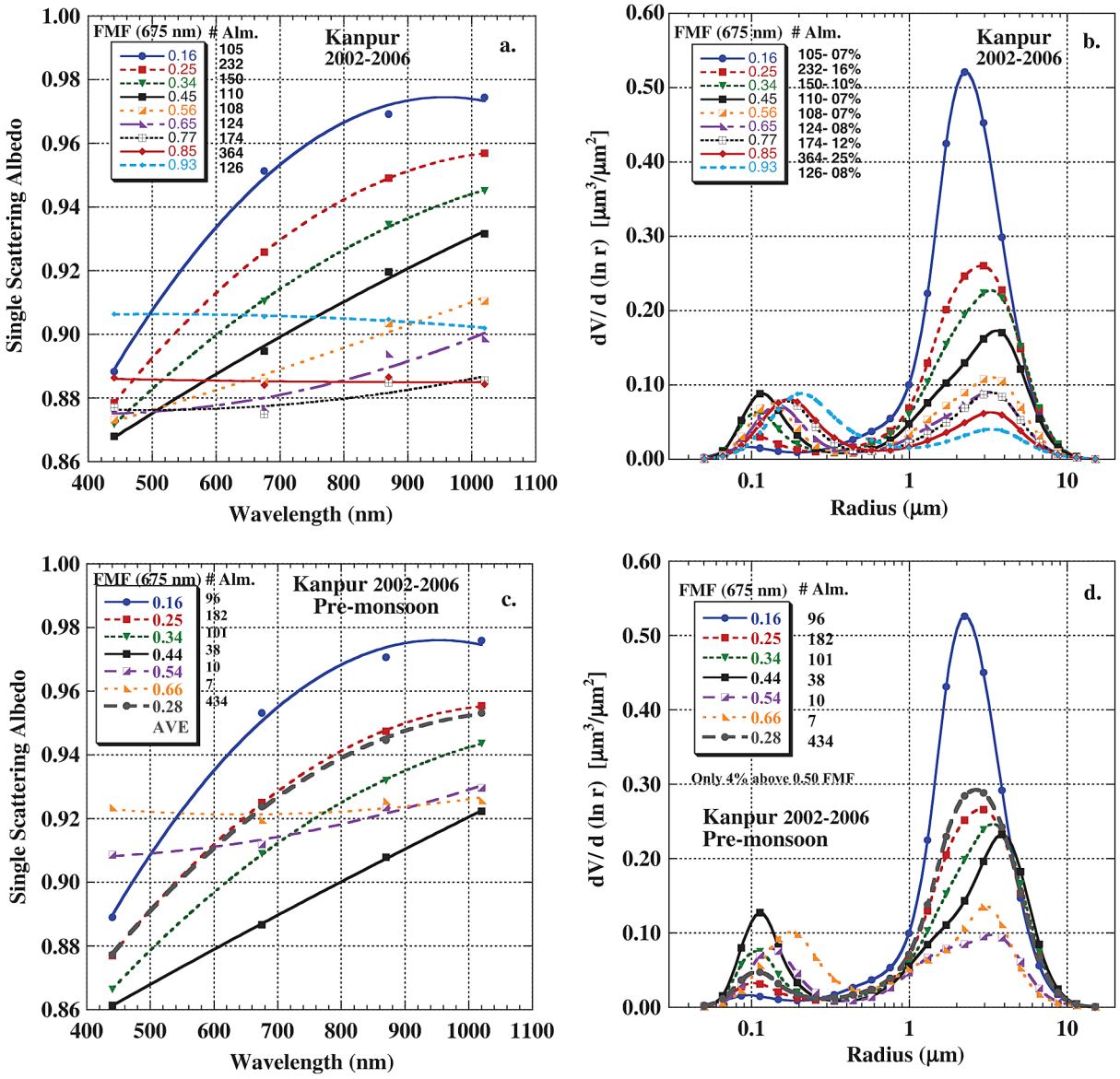

Figure 4. (a) Almucantar retrievals of spectral single scattering albedo averaged over multiple years for the complete range of fine mode fraction of AOD (675 nm) at Kanpur, for cases where AOD at 440 nm >0.4. (b) Similar to Figure 4a, but for the aerosol volume size distribution at Kanpur. (c) Similar to Figure 4a, but for the premonsoon season months of April, May, and June only in Kanpur. (d) Similar to Figure 4b, but for April, May, and June only.

almucantar scans to be robust samples (only a few days are represented). The premonsoon 3 month average SSA for Kanpur is ~0.88 at 440 nm, ~0.90 at 550 nm (midvisible), and ~0.95 in the near infrared wavelengths of 870 and 1020 nm. The magnitude of the effective total column aerosol absorption in northern India during the premonsoon season is very important in assessing the potential effect of aerosol on the monsoon circulation. Simulations by *Lau et al.* [2006], *Ramanathan et al.* [2005], and *Meehl et al.* [2008] all suggest that the high concentrations of strongly absorbing aerosols over India in the premonsoon months have a significant impact on the onset and strength of the monsoon circulation and resulting precipitation. Accurate knowledge of the magnitude of the aerosol absorption and AOD (both inferred from AERONET measurements) is critical for assessing these potential impacts.

[21] The SSA plotted as a function of FMF at 675 nm at Kanpur is shown in Figure 5. For all wavelengths, the SSA versus FMF is nearly linear for FMF values ranging from 0.16 to ~0.45 or 0.55. At FMF values > ~0.50, there is a reduction of slope, then a leveling off and finally an increase in SSA as FMF increases from 0.76 to 0.93. As previously discussed, the increase in SSA at the highest FMF levels is partly due to the increase in fine mode particle radius which increases the relative scattering efficiency. However, the nearly linear decrease in SSA from 0.16 to ~0.50 suggests that there may be relatively constant values of fine and coarse mode SSA that are combined in this range of

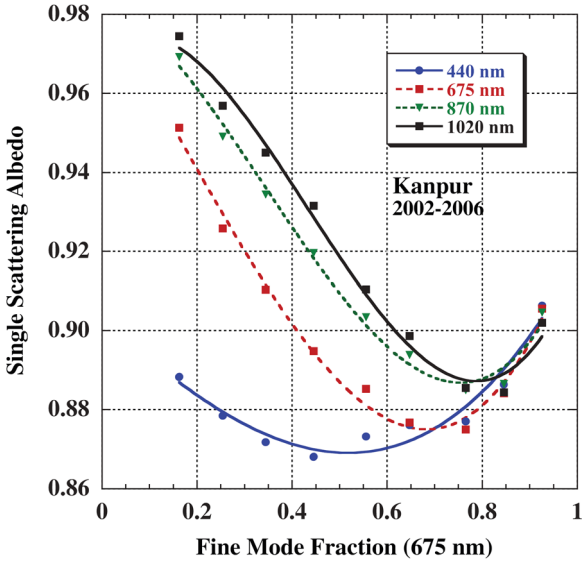

Figure 5. Spectral single scattering albedo as a function of the fine mode fraction of AOD (675 nm) at Kanpur.

FMF. Theoretically, if both the fine (SSA_{fine}) and coarse (SSA_{coarse}) single scattering albedo components remain constant then the total SSA of the mixture ($SSA_{Mixture}$) may be computed as a linear combination of the two weighted by the FMF of AOD by

$$SSA_{Mixture} = SSA_{fine}(FMF) + SSA_{coarse}(1 - FMF). \quad (1)$$

However, there are several probable reasons for nonlinearity of $SSA_{Mixture}$ variation as a function of FMF including (1) fine mode particle size and refractive indices are not static, resulting in variation in SSA_{fine}; for example, at higher FMF the fine particle radius increases resulting in higher SSA_{fine}; (2) fine mode particles may adhere to the surfaces of coarse mode dust particles (as observed in ACE-Asia) [*Arimoto et al.*, 2006] resulting in lower SSA_{coarse}; (3) some fine mode particles may be dust (not pollution) and therefore have a different SSA_{fine} than fine mode sulfate/BC/etc., mixed species particles; and (4) some coarse mode particles may not be dust (such as fly ash from coal combustion and/or emissions from briquette fuel made of coal dust and silt mixtures in China [*Yang et al.*, 2009]). It follows that the relatively linear trend in SSA for FMF <50% in Figure 5 does not necessarily suggest that this trend is due only to external mixtures of the two particle types however, since black carbon aerosol may adhere to the surface of dust particles and result in increasing absorption of the coarse mode itself. Some studies have in fact found evidence suggesting possible black carbon coating on dust particles in India [*Dey et al.*, 2008].

[22] The annual cycle of daily averages of SSA at 440 nm and the difference of 870–440 nm SSA at Kanpur are shown in Figure 6a. The spectral difference in SSA is an indicator of the relative magnitude of total aerosol absorption that occurs due to iron oxides in dust versus black carbon in fine mode aerosols [*Derimian et al.*, 2008a]. There is no strong seasonality to the 440 nm SSA; however, the 870–440 nm

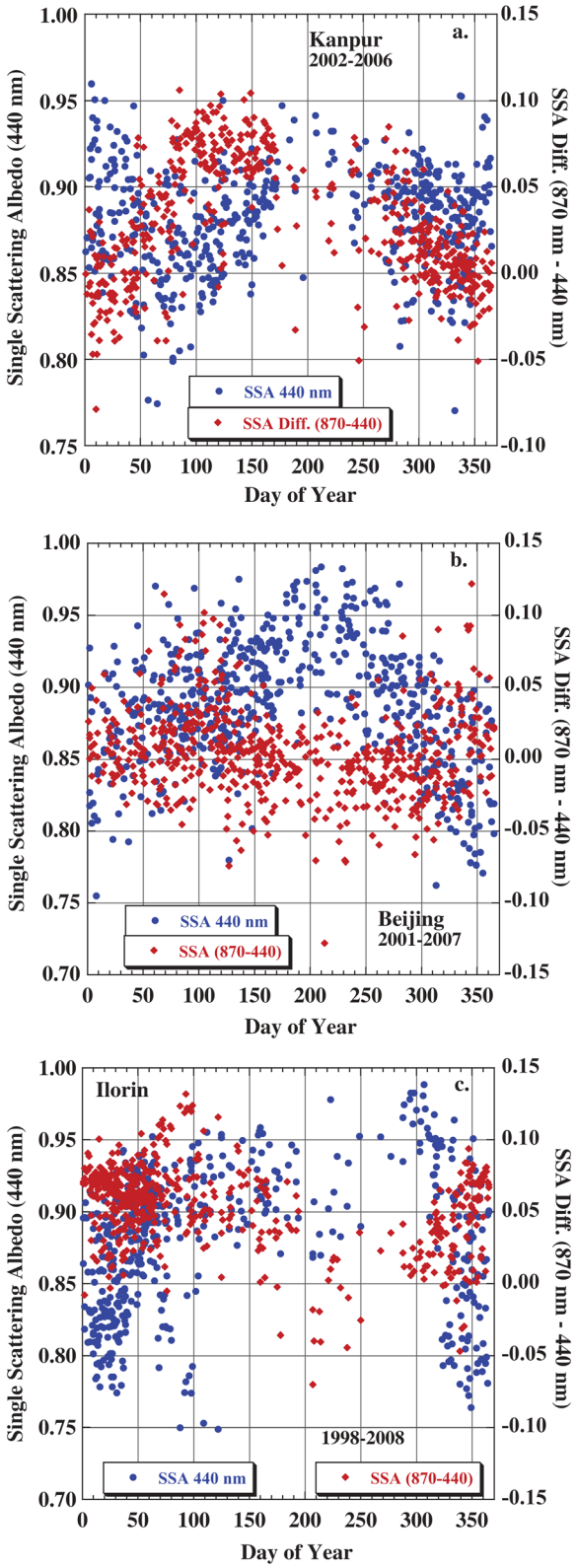

Figure 6. Daily average single scattering albedo (440 nm) and SSA difference (870–440 nm) versus day of the year, from multiyear monitoring at (a) Kanpur, (b) Beijing, and (c) Ilorin.

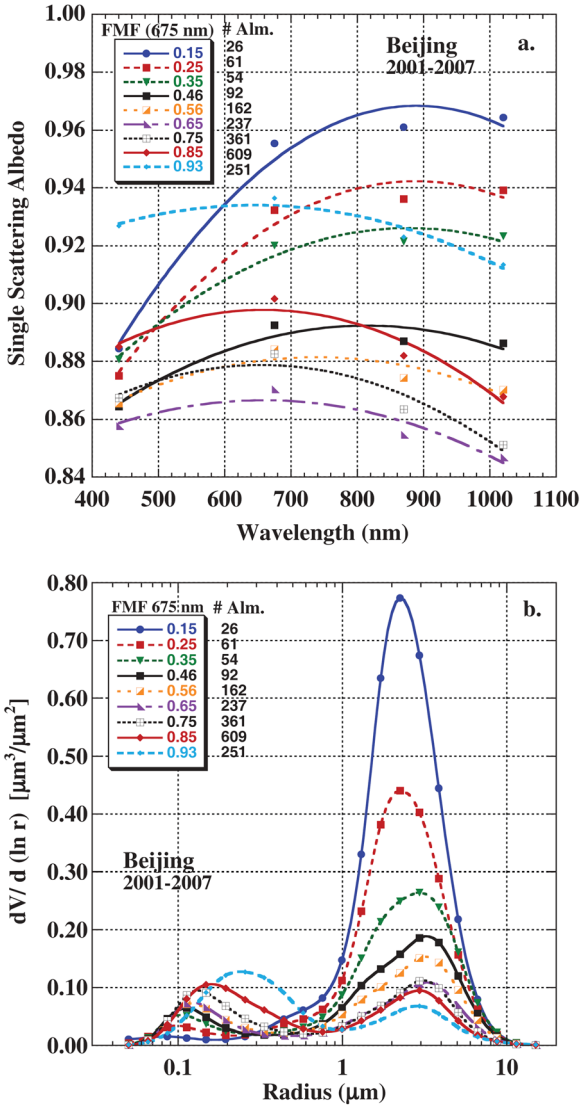

Figure 7. Similar to Figures 4a and 4b, but for Beijing.

SSA differences show a strong annual cycle. The 870–440 nm SSA differences which were less than or close to zero during the winter months suggest that the principal absorber in this season is black carbon. The greatest number of observations of large positive differences (>0.05) in SSA (870–440 nm) occurred during the spring dust season months of March through May, consistent with iron oxides in dust being the dominant absorber. In general there is an apparent opposing annual pattern of Angstrom exponent (Figure 2a) and 870–440 nm SSA difference in Figure 6a, due to the influence of dust on both particle size distribution and aerosol absorption. Note that there were very few almucantar retrievals made in the monsoon months of July–September due to the persistent high cloud fraction.

3.3.2. Beijing, China

[23] The relationships between both the averaged spectral single scattering albedo and size distributions over the range of fine mode fractions of AOD at 675 nm for Beijing are shown in Figure 7, from almucantar retrievals made during the period of 2001–2007 when AOD at 440 nm was higher than 0.4. These plots show several similarities to the relationships observed at Kanpur (Figure 4). At both Beijing and Kanpur the range of single scattering albedo at 440 nm as a function of FMF at 675 nm is relatively small. If the 0.93 FMF average is excluded, then the 440 nm ω_0 range is only ~0.03. As was the case in Kanpur, a major probable reason for the increase in SSA at the highest FMF values at all wavelengths is that the fine mode particle radius is significantly larger, resulting in greater scattering efficiency. In fact, for the 0.93 FMF bin the mean fine mode radius from 251 retrievals was 0.25 μm, while for FMF ranging from 0.25 to 0.65 the fine mode radius was much smaller ranging from ~0.14 to ~0.16 μm. At FMF of 0.93 the average AOD at 500 nm was 1.55, much higher than for the FMF range of 0.25–0.65 where the AOD at 440 nm varied from ~1.00 to 0.77. Therefore, the much higher AOD of fine mode aerosols at FMF of 0.93 likely resulted in greater coagulation rates at higher aerosol concentrations. Also since many of these highest FMF observations occurred during summer (discussed below) it is also likely that hygroscopic growth at high humidity also contributed to the fine mode particle growth. The retrieved imaginary part of the refractive index at 440 nm for FMF of 0.93 was ~0.011, while it was significantly higher at FMF of 0.65–0.85, ranging from ~0.017 to ~0.018, which is consistent with hygroscopic growth adding water to the fine particle composition. In situ ground-based measurements near Beijing in the summer of 2006 by *Cheng et al.* [2009] have found high values of SSA (~0.90–0.95 at 532 nm) during stagnant and polluted conditions even without taking hygroscopic growth into account (dry aerosol properties measured). They attribute the relatively low aerosol absorption to increased scattering due to submicron size particle growth from condensation and secondary particle formation that overwhelmed the enhancement in soot absorption by particle coating.

[24] The annual cycle of daily averages of SSA at 440 nm and the difference of 870–440 nm SSA at Beijing are shown in Figure 6b. The maximum values of 440 nm SSA occur from June through September (days ~150–270) when AOD, Angstrom exponent, and precipitable water are all at or near to annual maximum values (see Figure 2b). The 870–440 nm differences in SSA show more values less than zero than above in these summer months suggesting that the principal absorber in this season is black carbon. The largest number of observations of large positive differences (>0.05) in SSA (870–440 nm) occurred during the spring dust season months of March through May, consistent with iron oxides in dust being the dominant absorber. SSA differences exceeding 0.05 also occurred occasionally in the autumn and early winter suggesting a secondary season of dust events but with much less frequent occurrences compared to the spring season.

[25] From the Beijing almucantar database only about ~14% of the total retrievals showed dust domination, where FMF at 675 nm was less than 0.50. From Figure 2b, the Angstrom exponent seasonality graph shows that the minimum values occur in the months of March, April, and May, the spring dust transport season in Asia [*Huebert et al.*, 2003]. Therefore, in order to investigate the absorption properties when fine aerosol mixes with coarse mode dust, these three spring months were also analyzed separately. Figure 8 shows the single scattering albedo (all four wavelengths) as a

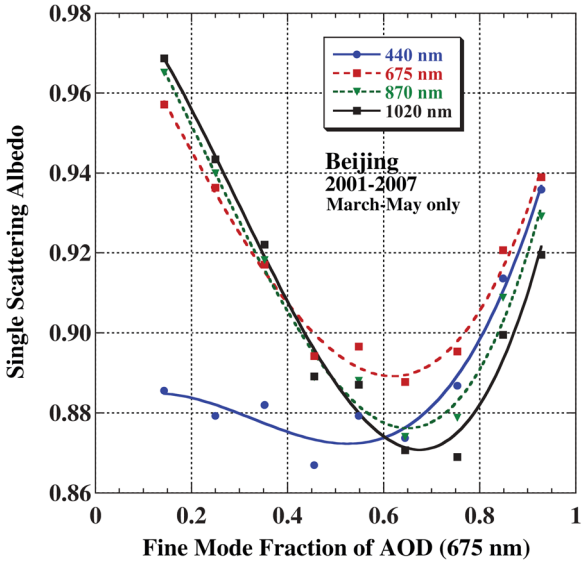

Figure 8. Average single scattering albedo as a function of the fine mode fraction of AOD (675 nm) at Beijing, for the spring season months of March, April, and May only.

function of the FMF of AOD at 675 nm at Beijing for the March–May spring dust season. Except for the 440 nm SSA that shows little change, the SSA at 675, 870, and 1020 nm all show relatively linear decreases as FMF increases for FMF values of <0.50, which is similar to Kanpur. This linear decrease in SSA as a function of FMF probably results from a combination of the linear mixture of fine and coarse components weighted by FMF of AOD (equation (1)) and is also possibly due to coarse mode particle coating by absorbing fine mode aerosols that contain black carbon. Much evidence of dust coating by fine particles has been shown for the East Asian region during the ACE-Asia campaign in spring of 2001. *Arimoto et al.* [2006] present scanning electron microscopy images showing black carbon particles adhering onto the surface of coarse mode dust, with typically ~15%–30% of the dust surface coated by black carbon which likely increases the absorption.

[26] *Yang et al.* [2009] made in situ ground-based measurements of aerosol single scattering albedo at Xianghe, China (~60 km east of the Beijing AERONET site) in March of 2006. Their measurements were made when ambient relative humidity was less than 40% on average and therefore aerosol hygroscopic growth was not a factor. From nephelometer data in conjunction with particle soot absorption photometer data they measured the 550 nm total (mixed) SSA of cases identified as dust to be 0.90, with the super micron particles having SSA of 0.94 while the submicron particles were more absorbing at 0.86. For these dust cases the scattering Angstrom exponent was found to be 0.59 and the fraction of scattering due to fine mode particles was 0.36 at 700 nm. For a similar FMF of AOD of 0.35 (also similar $\alpha_{440-870}$ = 0.57) the AERONET retrievals made during the March–May interval yield a total or mixed SSA of 0.90 at 550 nm, the same as the in situ data. Additionally the AERONET retrieved SSA interpolated to 550 nm for the most dust dominated FMF (bin average of 0.14) during March–May was ~0.925, similar to the 0.94 value measured in situ by *Yang et al.* [2009] for the coarse mode dust. The biomass burning and coal pollution SSA measured in situ by *Yang et al.* [2009] were 0.89 and 0.80, respectively, at 550 nm (with fine fraction of scattering at 700 nm of 0.65 and 0.70), while the AERONET retrieved SSA was 0.88 (interpolated to 550 nm) for a similar range of FMF of AOD for 0.65 to 0.75. Since coal pollution is much more likely to dominate regional haze in this region during spring, the SSA from in situ measurements seems to be significantly lower than from the AERONET retrievals for the fine mode dominated cases. However analysis by *Chaudhry et al.* [2007] at the same site suggests that surface measurements of aerosol properties are not always representative of column-integrated values due to vertical variability of aerosol and proximity to freshly emitted aerosol from various sources.

[27] Comparison of AERONET retrieved spectral SSA values between Beijing and Kanpur at low, mid, and high values of FMF of AOD at 675 nm (~0.15, ~0.45, and 0.85) is shown in Figure 9. The lowest FMF values (0.15) cases are from observations dominated by coarse mode desert dust events and the SSA at all four wavelengths agree to within 0.01 or less for these two sites. This suggests that on average there may be similar composition and perhaps similar amounts of iron oxides in the dust at these two locations, despite differing dust source regions. For the comparison at high FMF of 0.85, both Beijing and Kanpur had nearly equal SSA at both 440 and 870 nm, while differences at 675 and 1020 nm were ~0.015–0.02. At the intermediate FMF of 0.45, representative of mixed fine and coarse particle concentrations, the SSA at 440 and 675 nm were nearly equal (within ~0.01), while the difference at 870 nm was ~0.02 and at 1020 was ~0.035. The lower near-infrared SSA values at Beijing suggest that the coarse mode particles may be more absorbing there than in Kanpur, since the longer wavelengths are influenced more by coarse mode particle

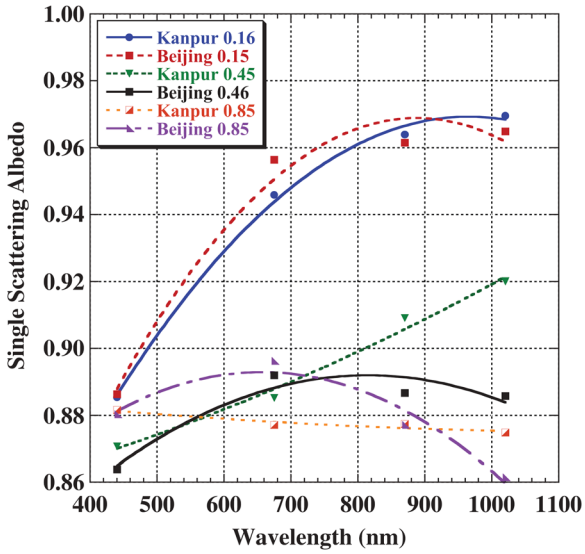

Figure 9. Comparison of spectral single scattering albedo at Beijing to Kanpur, for low (~0.15), mid (~0.45), and high (~0.85) fine mode fraction of AOD (675 nm).

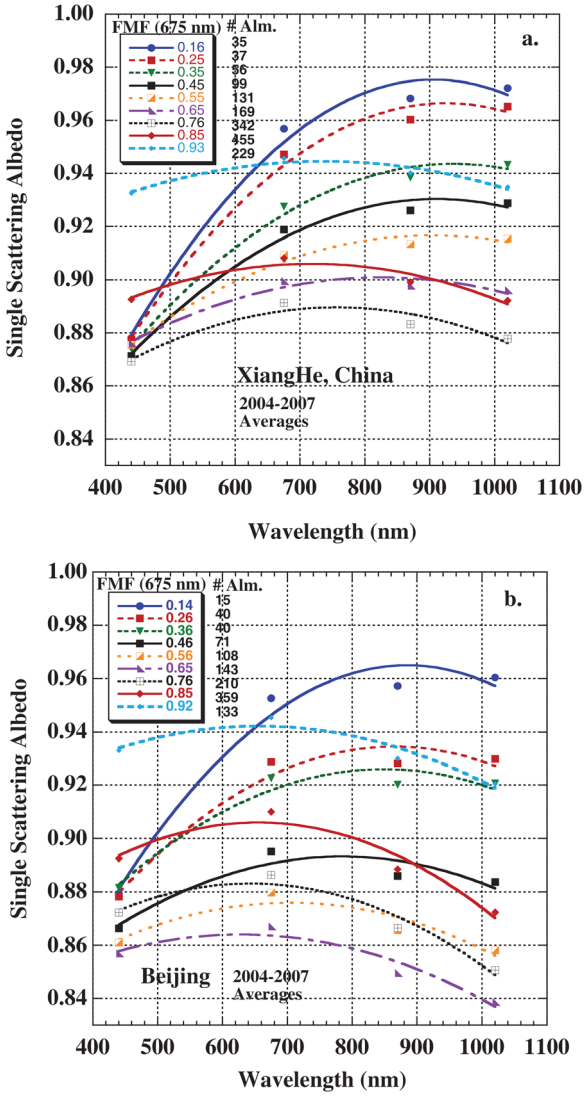

Figure 10. (a) Spectral single scattering albedo averaged over the years 2004–2007 for the complete range of fine mode fraction of AOD (675 nm) at XiangHe, China. (b) Similar to Figure 10a but for SSA at Beijing for 2004–2007.

scattering and absorption due to the FMF of AOD decreasing as wavelength increases. This greater near-infrared wavelength absorption in Beijing may result from a greater rate of black carbon coating of dust particles in Beijing versus Kanpur, resulting in different coarse particle absorption. Additionally, differences in fuel type between the regions may also account for differences in spectral absorption. *Yang et al.* [2009] describe a type of briquette commonly used in residential heating and cooking in China that is composed of a bound mixture of powdered coal and clay. The orange color of these briquettes, after the coal has burned, similar to the same color on the air sampling filters that *Yang et al.* [2009] collected from coal pollution led them to suggest that these particles may have significant iron oxide content. Therefore, the coarse mode particles in China may include particles other than dust and that are also coemitted with fine mode pollution, thereby further complicating the analysis of the fine and coarse mode mixtures.

[28] Retrievals of SSA from the AERONET site located in Xianghe, ~60 km east-southeast of Beijing, are shown in Figure 10 and compared to retrievals made in Beijing during the same time interval, 2004–2007. The XiangHe site is located in a relatively rural location as compared to the mega city of Beijing. For the highest and lowest FMF values of ~0.15 and ~0.92 the SSA for the two sites are very similar, differing by ~0.015 or less at all wavelengths. Therefore for strong dust events (average AOD at 440 nm was ~1.0 at both sites for FMF = 0.15) the SSA is almost equal, as expected, since the principal desert source regions (Takla Makan and Mongolian deserts) are almost equally distant from both sites. For the highest FMF observations (0.92 mean at 675 nm), the average AOD associated with these retrievals, ~1.55 at 440 nm, was the highest of any bin, and as seen in Figure 6b these retrievals of high SSA at 440 nm occur primarily in the summer when pollution aging and stagnation events are common. This combined with hygroscopic growth resulted in extremely high AOD levels over the extended region. Therefore, it may also be more likely that SSA under these conditions may be more regionally homogeneous. For the FMF bins of 0.25 through 0.75 the AOD at 440 nm is somewhat lower, but still high (averages from 0.80 to 0.84) allowing for very high sensitivity to aerosol absorption in the retrievals [*Dubovik et al.*, 2000]. Figure 11 shows a direct comparison between Beijing and XiangHe of the mean SSA values for FMF at 675 nm of 0.25, 0.45, and 0.65. At 440 nm, the SSA values are nearly equal at FMF of 0.25 and 0.45, while at 0.65 the SSA at Beijing is ~0.02 lower than at XiangHe. At the longer wavelengths of 675 through 1020 nm the differences in SSA are greater, ranging from ~0.02 to 0.06, with lower values at Beijing in all FMF cases. These lower SSA values at longer

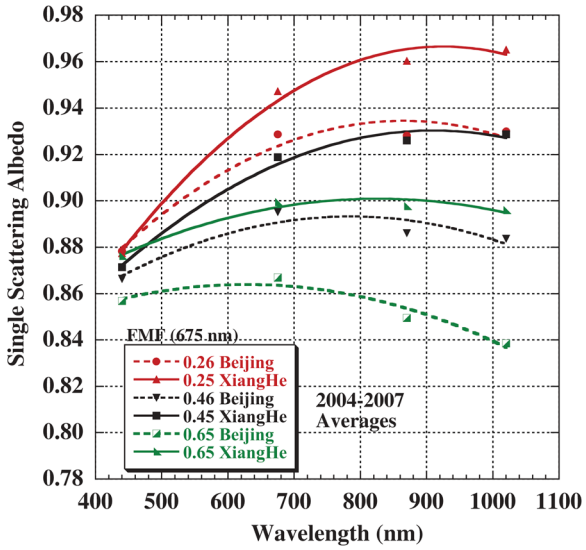

Figure 11. Comparison of spectral single scattering albedo at XiangHe to Beijing, for fine mode fraction of AOD (675 nm) of ~0.25, ~0.45, and 0.65 (all mixed mode cases).

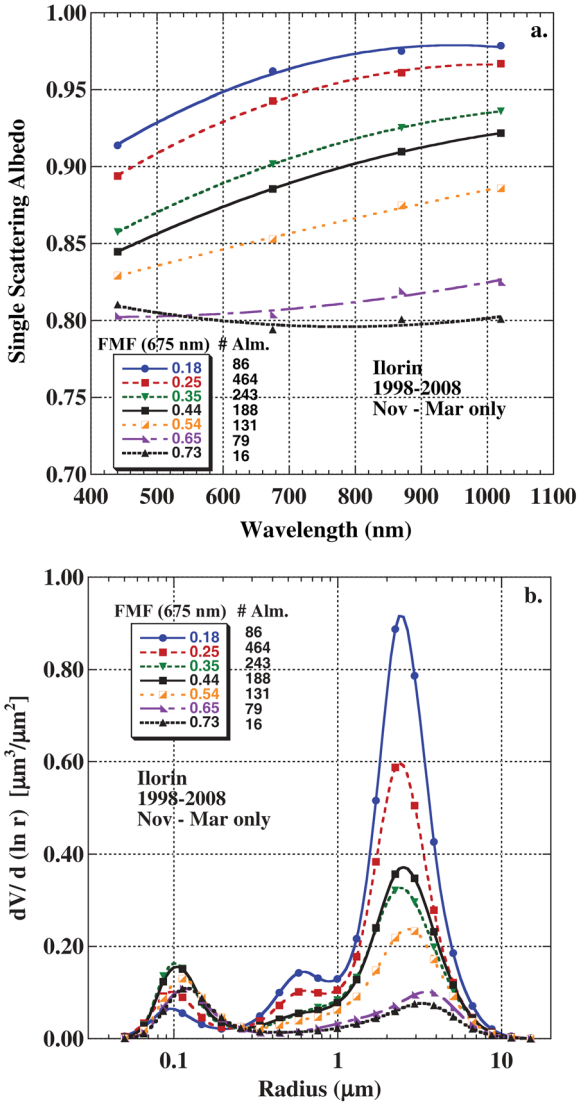

Figure 12. (a) Spectral single scattering albedo at Ilorin averaged over multiple years, during the biomass burning season only, for a range of fine mode fraction of AOD (675 nm). (b) Similar to Figure 12a but for the aerosol volume size distribution at Ilorin. Note that the maximum fine mode fraction bin is 0.73 at Ilorin due to a lack of high FMF observations.

wavelengths at Beijing (compared to relatively rural XiangHe) could be due to greater daily emission of absorbing coarse mode particles from the Beijing megacity; however, more detailed measurements including in situ data would be needed to investigate this possibility.

3.3.3. Ilorin, Nigeria

[29] The biomass burning season in West Africa occurs primarily from November through March. Therefore in Figure 12 we have limited the analysis to retrievals made in these months in order to study the mixing of North African savanna biomass burning aerosols with desert dust from the Sahara and Sahel regions. Significant differences can be noted when comparing Ilorin to either Kanpur or Beijing for the dynamics of both single scattering albedo and size distribution as a function of FMF. For single scattering albedo retrievals made over the range of FMF from ~0.18 to ~0.73 (the highest FMF observation bin at Ilorin), the range in 440 nm ω_0 values is very large at ~0.12, as compared to the relatively small range of ~0.02–0.03 at both Kanpur and Beijing over the same FMF range. This suggests that the fine mode biomass burning aerosols in West Africa are much more absorbing than the fine mode aerosols (primarily fossil fuel pollution and biofuels) in both Kanpur and Beijing. *Derimian et al.* [2008b] found a similar range of spectral SSA from AERONET data in Senegal (also West Africa) from January–March 2006 over a range of $\alpha_{440-870}$ from 0.11 to 0.92, which suggests that this is a widespread regional characteristic of aerosol absorption in West Africa. In situ measurements from aircraft of biomass burning aerosols in Niger (West Africa) in January and February 2006 by *Johnson et al.* [2008] also show very strong absorption for the fine mode aerosols. They estimated an average ω_0 at 550 nm of 0.81 (±0.05) for aged biomass burning aerosol, computed from observations where Angstrom exponent was higher than 1.0 (although some of the variability is due to mixing with dust aerosol). This is very similar to the interpolated average 550 nm ω_0 (~0.80) from the AERONET retrievals for the highest FMF observations (Figure 12a), which also include 27% coarse mode (likely dust) contribution to the AOD at 675 nm. This strong absorption attributed to smoke aerosol at Ilorin results in lower SSA values in the visible wavelengths than have been measured at any other biomass-burning site in the AERONET network [*Dubovik et al.*, 2002; *Eck et al.*, 2009], with the exception of smoke from episodic burning of Spinifex grasses in Australia [*Qin and Mitchell*, 2009]. This finding implies a high fraction of black carbon in the smoke from the Sahelian and Sudanian regions likely due to a greater percentage of flaming phase versus smoldering phase combustion, possibly due to a larger fraction of grass rather than woody fuels that are burned in the North African savanna environment [*Reid et al.*, 2005; *Eck et al.*, 2001].

[30] Another difference between the aerosol properties at Ilorin versus those at both Kanpur and Beijing is in the dynamics of the fine mode particle size distributions as a function of FMF. The fine mode particle size at Ilorin does not show much growth in radius as FMF increases as compared to the other two sites (Figure 12b). The median fine mode radius of the lognormal volume size distribution at Ilorin ranges from 0.13 to 0.16 μm for FMF ranging from 0.25 to 0.73 (with no trend in FMF), while the fine mode radius at Beijing varied from 0.14 to 0.25 μm for FMF of AOD at 675 nm ranging from 0.25 to 0.93. Possible reasons for a much smaller range in fine mode radius at Ilorin are the lower concentrations of fine particles there (note that the FMF maximum is much lower in Ilorin than in Beijing, 0.73 versus 0.93) and also that smoke aerosol is often much less hygroscopic than pollution aerosol, especially if there is a significant sulfate component present in the pollution [*Kotchenruther and Hobbs*, 1998]. The relationship of spectral SSA as a function of FMF at Ilorin is shown in Figure 13. For all four wavelengths, the SSA shows a more linear relationship versus FMF than either Beijing or Kanpur to a higher value of FMF (up to ~0.75 FMF at Ilorin) likely due in part to the more static fine mode particle size at Ilorin. A unique feature of the size distributions of the coarse mode

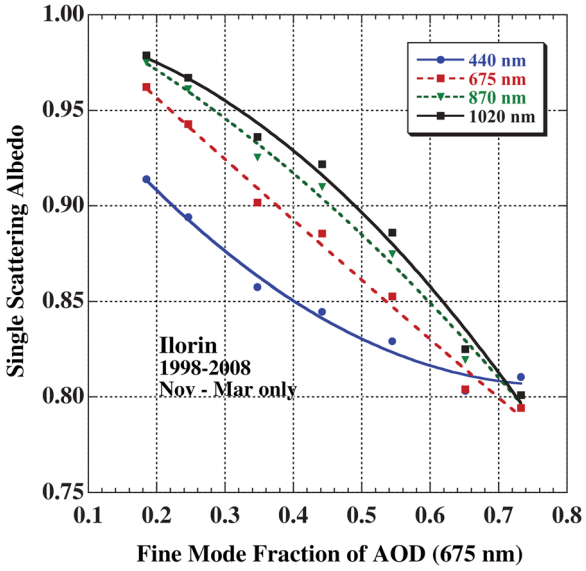

Figure 13. Average single scattering albedo as a function of the fine mode fraction of AOD (675 nm) at Ilorin, for the biomass burning season months of November through March (5 months).

dominated cases at Ilorin (Figure 12b) is the presence of a middle size mode at ~0.6 μm radius in the lowest FMF bins. This middle size mode has not been observed at any other AERONET sites in version 2 retrievals of dust observations, and we will discuss this in more detail below.

[31] *Johnson et al.* [2009] compared in situ measured aerosol optical properties from an aircraft vertical profile flight over the Banizoumbou (Niger) AERONET site on 19 January 2006. This was a mixed aerosol case with Angstrom exponent (450–700 nm) of ~0.8–0.9 and high 550 nm AOD of ~0.75, where a shallow dust layer up to 1 km altitude was overlain by a layer of predominantly fine mode smoke. Both aircraft and AERONET measurements of column integrated AOD at 550 nm and of α were in good agreement for this case, with $\Delta\tau$ = 0.08 and $\Delta\alpha$ = 0.06, suggesting that both were sampling the same aerosol mixture. The aircraft measured column-mean SSA at 550 nm (from PSAP and nephelometer) was 0.87, in good agreement with the AERONET retrieval of 0.85 (interpolated to 550 nm). Since relative humidity was typically ~40% and never higher than 70% there was no need to account for the effects of aerosol hygroscopic growth on scattering and absorption. *Osborne et al.* [2008] compared three cases of aircraft flights (on three different days) over the same site during the same experiment with the same instruments and aircraft but found that the aircraft in situ measured SSA values ranged from 0.04 to 0.07 higher than the AERONET version 2 retrievals. However, for all three of these cases the aircraft measured Angstrom exponents were found to be ~0.40 lower than the AERONET measured values. This discrepancy in α suggests that the aircraft may have sampled a different fine and coarse mode fraction mixture than the column integrated value measured by AERONET, and the higher SSA in conjunction with lower α measured by the aircraft is consistent with this possibility. In fact, for the linear fit of SSA versus α for all aircraft data from DABEX, reported in the work of *Johnson et al.* [2008], a difference of 0.40 in α corresponds to a difference in SSA of ~0.06, almost the same value of the bias reported in *Osborne et al.* [2008].

[32] A comparison of the SSA at 550 nm versus Angstrom exponent for the DABEX in situ measurements [after *Johnson et al.*, 2008] versus the multiyear means at Ilorin for the biomass burning season months (November–March) is shown in Figure 14. The Angstrom exponent from the aircraft measurements was computed from nephelometer scattering coefficient measurements from 450 to 700 nm data. To closely match the Angstrom exponent of the aircraft data, we computed the total column scattering optical depth at 440 and 670 nm from the AERONET retrievals and computed the scattering Angstrom exponent from these wavelengths, which are very similar to the nephelometer wavelengths. The scattering optical depths were computed by subtracting the spectral absorption optical depths from extinction optical depths, with the SSA utilized to compute the absorption optical depths by

$$\tau_{abs} = (1 - \mathrm{SSA}) \times \tau_{ext}. \quad (2)$$

The aircraft flights (93 total flight runs) were made during January and February 2006 during the DABEX experiment [*Haywood et al.*, 2008] over three countries in West Africa: Nigeria, Niger, and Benin. The AERONET data are from one site in Nigeria (Ilorin) from multiple years, from the period 1998 to 2008. The number of almucantar scans averaged per scattering Angstrom exponent (SAE) bin ranged from >300 scans for both the 0.11 and 0.29 SAE bins to only 22 and 6 for the 1.47 and 1.70 SAE average bins, respectively. There were very few observations of biomass burning dominated cases (when SAE is high) since some level of desert

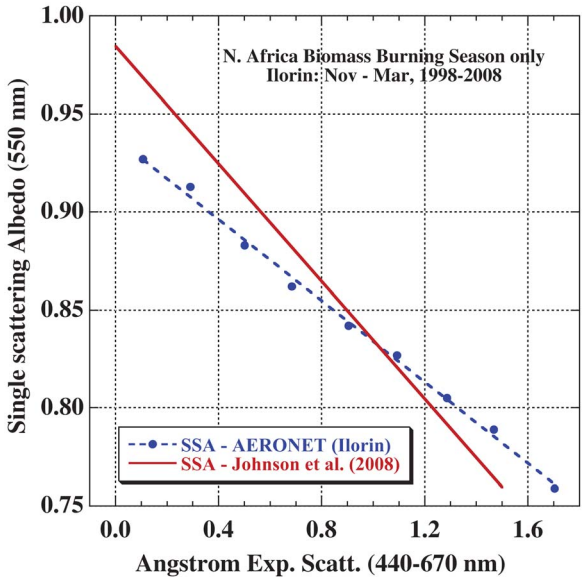

Figure 14. Comparison of single scattering albedo at 550 nm versus scattering Angstrom exponent (440–675 nm for AERONET and 450–700 nm for in situ) for multiyear averages derived from Ilorin AERONET retrievals to means from in situ aircraft measurement runs in Nigeria, Niger, and Benin during the DABEX campaign of January through February 2006 [from *Johnson et al.*, 2008].

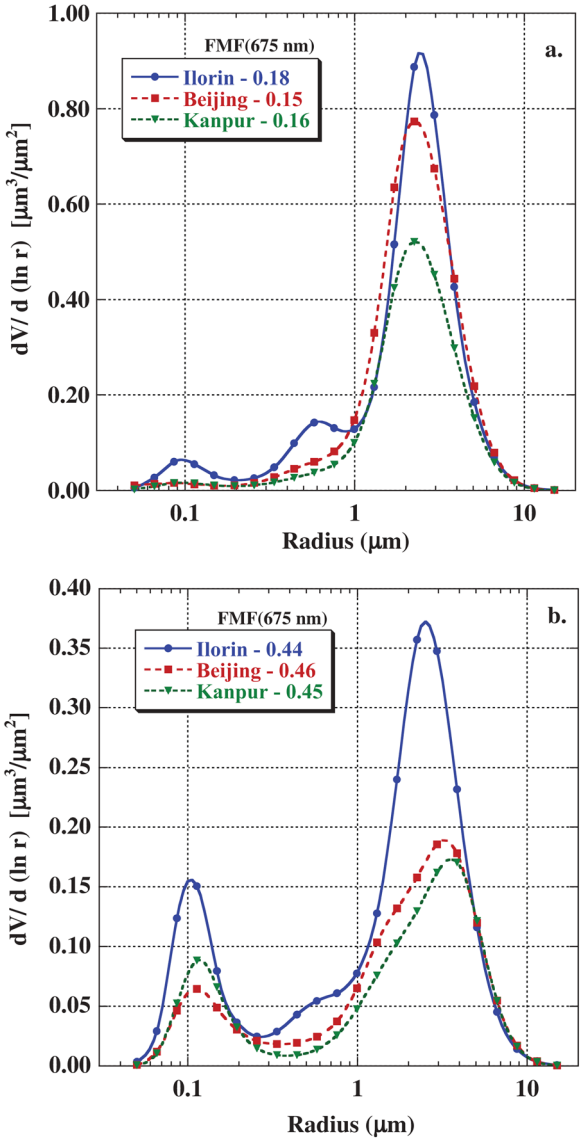

Figure 15. Comparison of aerosol volume size distributions from Ilorin, Kanpur and Beijing at fine mode fractions of (a) ~0.16, dust dominated and (b) ~0.45, mixed mode cases. Note the middle mode (centered at ~0.6 μm) present at Ilorin that was not observed at the other sites.

dust was pervasive at this site. This comparison cannot be considered a validation, but it does provide a sense of the agreement in "climatological" values of SSA as a function of Angstrom exponent between in situ measurements and remotely sensed retrievals. The best fit line to the DABEX aircraft run data (from Figure 12 of *Johnson et al.* [2008]) is shown in comparison to the SSA interpolated to 550 nm from the averaged almucantar data (Figure 14). The AERONET retrieved SSA is remarkably linear as a function of Angstrom exponent over the entire range of $\alpha_{440-670}$ from 0.11 to 1.70. The slope of the AERONET retrieved SSA versus Angstrom is found to be less than that of the aircraft measured data. However, *Johnson et al.* [2008] stated that the in situ measured SSA of the dust dominated aircraft runs during DABEX may be overestimated by 0.01–0.02 due to instrumental losses of large particles in the PSAP instrument, resulting in an underestimation of absorption. If it can be assumed that the aircraft measured SSA at $\alpha_{450-700}$ of zero is ~0.015 or 0.02 too high due to this issue, then the difference between the AERONET retrievals and DABEX in situ measured SSA would be ~0.02 or less over the entire range of Angstrom exponents that are common to both data sets.

[33] The annual cycle of daily averages of SSA at 440 nm and the difference of 870–440 nm SSA at Ilorin are shown in Figure 6c. A very large range in 440 nm SSA values occur during the burning season months of November–March, with some days where absorption is dominated by dust (relatively high SSA) some by biomass burning (low SSA) and many days where there are intermediate values that suggest mixtures. The 870–440 nm differences in SSA show more values near to and less than zero in the summer months suggesting that the principal absorber in this season is black carbon. Trajectory analyses, using the NOAA HYSPLIT model, in this season for days when retrievals were made suggest that the source of these aerosols may be biomass burning in the forested regions of central equatorial Africa and from the oil and natural gas production fields in the Niger delta region, where the greatest amount of gas flaring in the world occurs. These summer months also have very few days where retrievals were made due to the high cloud fraction associated with the high monsoon rainfall.

[34] As previously mentioned, a midsize aerosol mode was present in the dust and mixed fine/coarse mode aerosol retrievals at Ilorin. Figure 15 shows a comparison of Ilorin size distributions to both Kanpur and Beijing, for dust dominated cases (FMF ~ 0.16) and mixed aerosol cases (FMF ~ 0.45). For both the dust and mixed aerosol cases there is a middle mode at Ilorin (mode maximum at ~ 0.6 μm) that is minimal or absent in the other two sites. This middle mode is also absent from other dust dominated size distributions from AERONET retrievals made at sites in the Middle East and Africa [*Dubovik et al.*, 2002; *Eck et al.*, 2008]. This finding suggests the possibility of a somewhat unique source for aerosols that are transported over Ilorin. The Bodele Depression of central Chad (in the southern Saharan desert) is upwind at times of Ilorin and is sometimes described as the single largest individual desert dust source on Earth. From the Bodele Dust Experiment (BoDEx) in 2005, *Todd et al.* [2007] found that the dust in this region consists predominantly of fragments of diatomite sediment from fossil diatoms deposited in a very large paleolake bed [*Bristow et al.*, 2009]. A scanning electron microscopy (SEM) image of a dust sample from the Bodele in the work of *Todd et al.* [2007] show fragments of diatoms of various sizes, suggesting a possible source of midsized particles. Additionally, a CIMEL instrument deployed in the Bodele Depression in 2005 as a part of the BoDEx experiment also showed this middle mode in the AERONET size distribution retrievals [*Todd et al.*, 2007].

[35] AERONET retrievals of trimodal size distributions have been very unusual throughout most of the history of the network and at nearly all sites. An exception was at the beginning of AERONET measurements in 1993 when Mt. Pinatubo volcanic sulfate aerosols were present in the stratosphere [*Holben et al.*, 1996]. Size distribution retrievals made in late June 1993 at sites in both North America

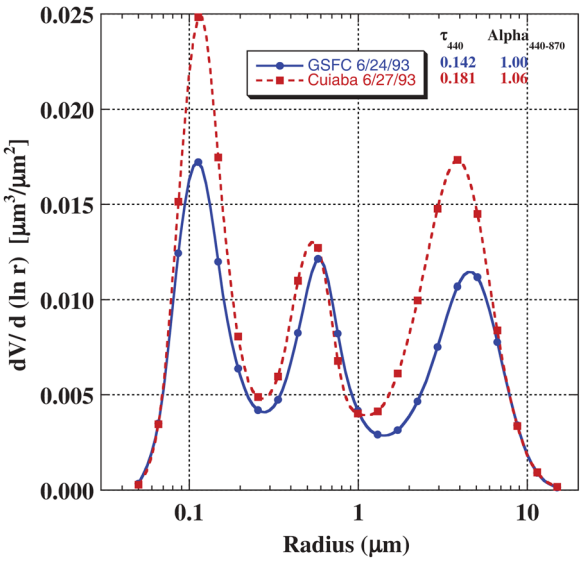

Figure 16. Aerosol volume size distribution retrievals from the GSFC, USA and Cuiaba, Brazil AERONET sites in June 1993, when Pinatubo volcanic aerosol was present in the stratosphere. Note the similarity in the middle mode (~0.6 μm) between sites, which is nearly equal in particle size to other measurements of aged Pinatubo aerosols (see text in section 3.3.3).

(GSFC, USA) and South America (Cuiaba, Brazil) are shown in Figure 16. A clearly defined middle mode is present at both sites of nearly equal magnitude and radius. The Pinatubo eruption occurred two years earlier in June 1991 and the concentrations of volcanic aerosols had decreased significantly by 1993 from the peak values that occurred in the months immediately after eruption. The middle mode peak of ~0.56 μm radius of the volume size distribution at both AERONET sites is found to be consistent with retrievals made by *Asano et al.* [1993], using spectral AOD measurements from January–April 1992, of 0.6 μm volume radius. Similarly, in situ stratospheric sampling (impactor) from aircraft in March 1992 yielded an effective radius of 0.53 μm [*Pueschel et al.*, 1994]. The close agreement in AERONET retrievals of the Pinatubo aerosol size with other measurements suggests that AERONET retrievals are sensitive to the occurrence of middle mode size aerosols in the presence of both accumulation (fine) and coarse mode aerosols.

3.4. Climatologies of Absorption Angstrom Exponent as a Function of FMF

[36] The absorption Angstrom exponent (AAE) is computed similarly to the traditional Angstrom exponent but with absorption aerosol optical depth (AAOD) instead of extinction aerosol optical depth. The value of the AAE is determined primarily by the dominant type or mixture of absorbing constituents in the aerosol. It is often assumed that black carbon has a constant imaginary index of refraction from the visible through near infrared wavelengths [*Bergstrom et al.*, 2002]. In the case of aerosol dominated by fine mode sized particles with black carbon as the only absorbing species present, the value of AAE would equal 1 [*Bergstrom et al.*, 2007]. In fact both in situ and remote sensing measurements have yielded AAE values from ~1 to 1.2 for pollution aerosol off of the east coast of the United States [*Bergstrom et al.*, 2007], suggesting that black carbon was the principal absorber. Mineral dust aerosol with absorption due to iron oxides, which is stronger in the UV and short wavelength visible wavelengths and decreases into the near infrared, would be expected to have AAE much greater than 1, and *Bergstrom et al.* [2007] present data of long distance transported Saharan dust (in Puerto Rico during the PRIDE experiment) that had an AAE of ~2.3. Although organic carbon is weakly absorbing in comparison to black carbon, it also exhibits stronger absorption in the UV and short wavelength visible that can result in higher values of AAE. In laboratory experiments *Lewis et al.* [2008] found that weakly absorbing biomass burning smoke had an AAE as high as 2.5 (532–870 nm) while strongly absorbing smoke had AAE values approaching 1. For high AOD smoke hazes in Alaska of weakly absorbing smoke (SSA ~ 0.97), *Eck et al.* [2009] computed AAE values of ~2 while for strongly absorbing smoke in Zambia (SSA at 550 nm ~ 0.86) they computed an average AAE of ~1.3, both from AERONET retrievals.

[37] Absorption aerosol optical depths $\tau_{abs\lambda}$ were computed from extinction optical depths and SSA as in equation (2) for three wavelengths: 440, 675, and 870 nm. The AAE was then computed in a similar fashion to the extinction Angstrom exponent as the negative of the slope of the $\ln\tau_{abs\lambda}$ versus $\ln\lambda$ (as a regression fit to the three wavelengths). In Figure 17, the climatologies of absorption aerosol optical depths, for retrievals where $\tau_{a440} > 0.4$, as a function of FMF of AOD at 675 nm are presented for the AERONET sites that are the focus of this study. The AAE for Kanpur (Figure 17a) varies from 2.14 for the most coarse mode dust dominated observations (FMF = 0.16) to 1.29 for the most fine mode dominated cases (FMF = 0.93). For approximately equal contributions of fine and coarse mode aerosol to the AOD at 675 nm (FMF of 0.45 and 0.56) the average AAE was ~1.5. A very similar range of AAE was observed at Ilorin (Figure 17b), with coarse dust dominated (FMF = 0.18) average of 2.10, and for the highest FMF of AOD at Ilorin, 0.73 at 675 nm, the AAE was 1.37, which is nearly equal to the AAE retrieved at Kanpur for a similar FMF. The AAE computed by *Bergstrom et al.* [2007] for Saharan dust of 2.34 is similar to the values determined from AERONET retrievals for coarse mode dust at Kanpur and Ilorin. For both Kanpur and Ilorin it is also noted that the three wavelengths of $\tau_{abs\lambda}$ are well fit by a linear regression line in logarithmic coordinates. *Bergstrom et al.* [2007] also found a generally linear fit of ln $\tau_{abs\lambda}$ versus $\ln\lambda$ from the UV through 1 μm range for several aerosol types including desert dust, biomass burning, and pollution. *Eck et al.* [2009] also showed very linear $\tau_{abs\lambda}$ versus $\ln\lambda$ for both very absorbing smoke in Zambia and very weakly absorbing smoke in Alaska.

[38] In China however, there is an interesting departure from linearity in the relationship of ln $\tau_{abs\lambda}$ versus $\ln\lambda$, at both the Beijing and XiangHe AERONET sites. For both of these sites the computed AAE are much larger for the 440–675 nm wavelength range than for the 675–870 nm interval (Figures 17c and 17d). The AAE values for the 675–870 nm wavelength interval are quite low, with values in Beijing

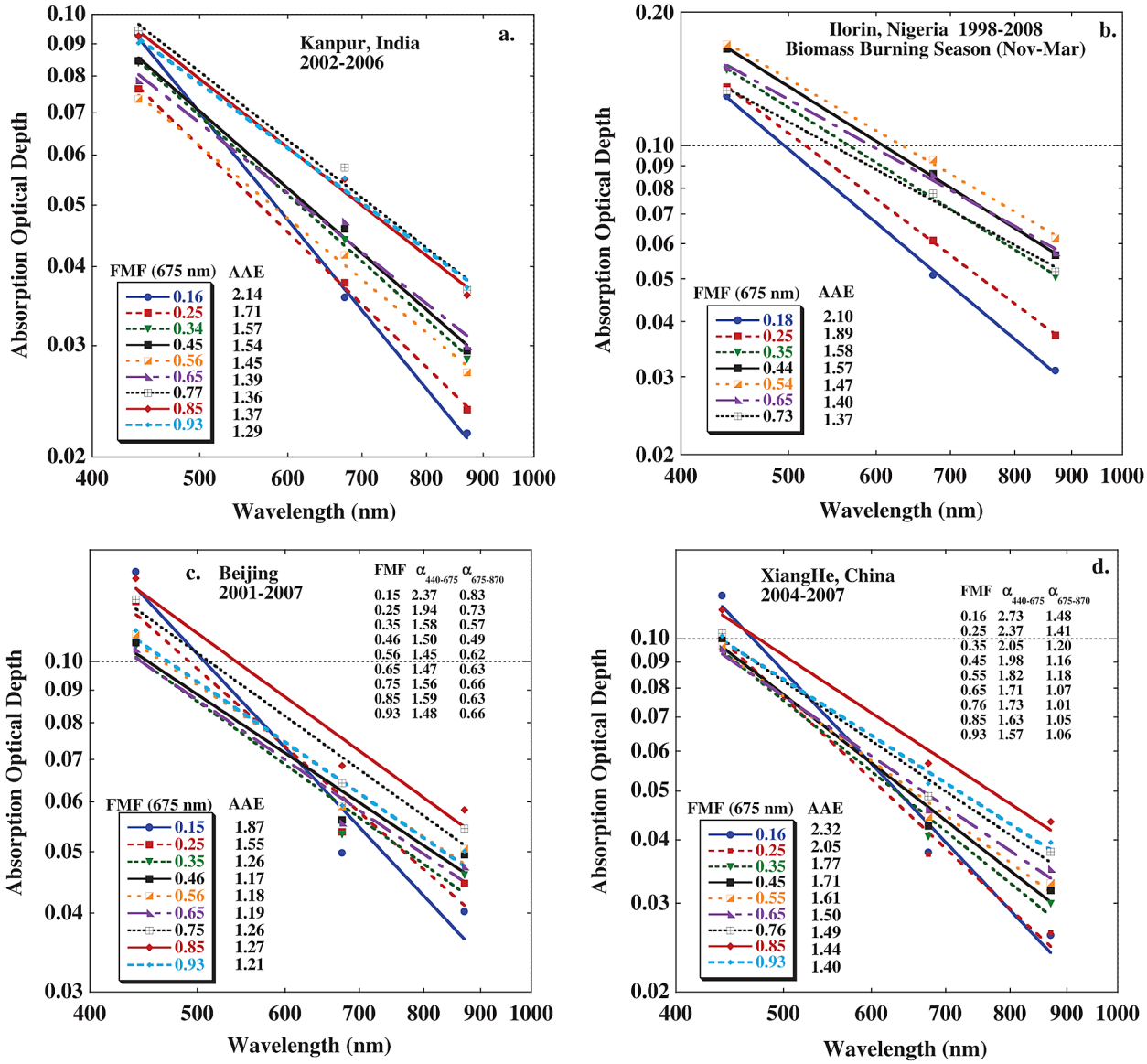

Figure 17. Average spectral aerosol absorption optical depths versus wavelength in logarithmic coordinates for the complete measurement range of fine mode fraction of AOD (675 nm) for (a) Kanpur, (b) Ilorin, (c) Beijing, and (d) XiangHe.

less than 1.0 for all FMF values and as low as 0.49, which is well below the typically assumed lower limit of 1 for black carbon. The range of AAE values at both sites in China for the 440–675 nm wavelength interval are similar to those observed at Kanpur and Ilorin (for the 440 nm to 870 nm interval) and similar to values derived from measurements reported by *Bergstrom et al.* [2007]. Therefore, it seems as though the $\tau_{abs\lambda}$ at 870 nm may be anomalously high perhaps resulting from strongly absorbing coarse mode particles that may be unique to China. In fact, measurements made by *Chaudhry et al.* [2007] at XiangHe in 2005 did show very strong absorption by the coarse mode. This apparently anomalous nonlinearity in AAE for the AERONET sites in China needs to be verified further with other types of measurements, both in situ and remote sensing. We do not have information on individual particle types and absorption to investigate this apparently atypical wavelength dependence of $\tau_{abs\lambda}$; therefore, further analysis of this issue is beyond the scope of this study.

4. Summary and Conclusions

[39] Mixtures of coarse mode dust with fine mode combustion generated aerosols (fossil fuel and biomass burning) were investigated in three locations that are in and/or downwind of major global aerosol emission source regions. Multiyear monitoring at AERONET sites in Beijing (central eastern China), Kanpur (Indo-Gangetic Plain, northern India), and Ilorin (Nigeria, Sudanian zone of West Africa) allowed for a climatological characterization of aerosol optical properties. Improved understanding of aerosol optical properties, especially absorption is critical to a better understanding of the aerosol related effects in these regions.

[40] 1. Multiyear climatological averages of spectral single scattering albedo versus fine mode fraction of AOD at 675 nm at all three sites (Kanpur, Beijing, and Ilorin) exhibited relatively linear trends up to ~50% FMF. This suggests the possibility that external linear mixing of both fine and coarse mode components (weighted by FMF), where the SSA of each component remains relatively constant for this range of FMF only, dominates the SSA variation. However, it is likely that a combination of other factors is also involved in determining the dynamics of SSA as a function of FMF, such as fine mode particles adhering to coarse mode dust.

[41] 2. Relatively small dynamic ranges of SSA at 440 nm (~0.03 or less) were observed for most FMF's less than ~0.80 at Kanpur and both Beijing and XiangHe, suggesting that the magnitude of absorption for fine mode aerosols (due to black carbon) and coarse mode dust (due to iron oxides) is similar at these sites in the short wavelength visible region. This contrasts with relatively large dynamic variation of SSA at 675 nm through 1020 nm, ranging from ~0.07 to ~0.12 (lower for 675 nm and highest at 1020 nm) for the same FMF range. The small variation in SSA at 440 nm at these sites suggests an advantage in satellite retrievals of AOD at 440 nm or other wavelengths at the short end of the visible range, since SSA must either be assumed a priori in many satellite retrieval algorithms or the ability to retrieve absorption magnitude is relatively weak.

[42] 3. Conversely, at Ilorin, Nigeria a relatively large dynamic range in 440 nm SSA (~0.12) as a function of either FMF or Angstrom exponent was observed. This is primarily due to much more absorbing fine mode aerosol (from savanna biomass burning) that is also relatively static in radius and of smaller size as compared to the fine mode pollution aerosols in both Kanpur and the Beijing region.

[43] 4. The XiangHe AERONET site is located ~60 km east southeast of Beijing in a relatively rural area. Both XiangHe and Beijing showed relatively similar spectral SSA (within ~0.015) at all wavelengths for both the most dust-dominated cases (FMF ~ 0.15) and the most predominantly fine mode-dominated pollution cases (FMF ~ 0.93). However, for mixtures of fine and coarse aerosols, Beijing showed lower SSA than XiangHe for the 675 through 1020 nm wavelength range (~0.02 to ~0.06 lower) for FMF values ranging from ~0.20 to ~0.70. The lack of significant SSA difference at 440 nm between these two sites combined with increasingly greater differences as wavelength increased suggests that possibly there was some component of the coarse mode aerosol that was more absorbing at the Beijing site during mixed fine-coarse aerosol events.

[44] 5. A comparison of in situ and AERONET measurements of SSA at 550 nm as a function of Angstrom exponent was made between the AERONET climatology at Ilorin and aircraft in situ measurements made during the DABEX experiment in January–February 2006 in Nigeria, Niger, and Benin. The SSA from AERONET at Ilorin was very linear as a function of scattering Angstrom exponent for the entire $\alpha_{440-670}$ range of 0.1–1.7. If the SSA of the aircraft dust runs were assumed to be overestimated by 0.01–0.02 (as suggested by *Johnson et al.* [2008]), then the agreement between the best fit line of the aircraft data to the AERONET retrieved SSA would be within ~0.02 or less for the entire coincident range of Angstrom exponent. Although this is not a validation or direct comparison (since measurements are not space and time coincident) it does suggest that there is a close agreement in regional characterization of mean SSA in West Africa between in situ measurements and AERONET retrievals over a wide range of fractional mixtures of biomass burning smoke and desert dust.

[45] 6. The ω_0 at Ilorin from the AERONET retrievals for the highest FMF observations (dominated by biomass burning aerosols) range from ~0.81 to 0.80 in the visible wavelengths which also include ~25% coarse mode (likely dust, which is less absorbing) contribution to the AOD at 675 nm. This strong absorption attributed to smoke aerosol at Ilorin results in lower SSA values in the visible wavelengths than have been regularly measured at any other biomass-burning sites in AERONET. This finding suggests a high fraction of black carbon in the smoke aerosol emitted from the Sahelian and Sudanian regions likely due to a greater percentage of flaming versus smoldering phase combustion, probably from a larger fraction of grass versus woody fuels that were burned.

[46] 7. The spectral variation of the climatological averaged aerosol absorption optical depth was nearly linear in logarithmic coordinates over the wavelength range of 440–870 nm for both the Kanpur and Ilorin sites. For these two sites the absorption Angstrom exponents (AAE) varied from ~2.1 for coarse dust at FMF of ~0.17 to AAE of ~1.35 for predominantly fine mode aerosols at FMF of ~0.75 and higher. However, at both sites in China (Beijing and Xianghe), a distinct nonlinearity in spectral AAOD in logarithmic space was observed, suggesting the possibility of anomalously strong absorption in coarse mode aerosols increasing the 870 nm AAOD. However, this hypothesis needs to be investigated with other data including in situ measurement techniques.

[47] **Acknowledgments.** The AERONET project was supported by Michael D. King, retired in 2008 from the NASA EOS project office, and by Hal B. Maring, Radiation Sciences Program, NASA Headquarters. S. N. Tripathi acknowledges support from Department of Science and Technology, ICRP and Indian Space Research Organisation GBP programmes. S. N. Tripathi was also supported in part by appointment to the NASA Postdoctoral Program at Goddard Space Flight Center, administered by Oak Ridge Associated Universities through a contract with NASA. The authors are indebted to Harish Vishwakarma for his efforts in the operation of Kanpur AERONET instruments and to ISRO-GBP for financial support to R.P. Singh through a research project.

References

Arimoto, R., et al. (2006), Characterization of Asian dust during ACE-Asia, *Global Planet. Change*, *52*, 23–56.

Asano, S., A. Uchiyama, and M. Shiobara (1993), Spectral optical thickness and size distribution of the Pinatubo volcanic aerosols as estimated by ground-based sunphotometry, *J. Meteorol. Soc. Jpn.*, *71*, 165–173.

Bergstrom, R. W., P. B. Russell, and P. Hignett (2002), Wavelength dependence of the absorption of black carbon particles: Predictions and results from the TARFOX experiment and implications for the aerosol single scattering albedo, *J. Atmos. Sci.*, *59*, 567–577.

Bergstrom, R. W., P. Pilewskie, P. B. Russell, J. Redemann, T. C. Bond, P. K. Quinn, and B. Sierau (2007), Spectral absorption properties of atmospheric aerosols, *Atmos. Chem. Phys.*, *7*, 5937–5943.

Bond, T. C., and R. W. Bergstrom (2006), Light absorption by carbonaceous particles: An investigative review, *Aerosol Sci. Tech.*, *40*, 27–67.

Bristow, C. S., N. Drake, and S. Armitage (2009), Deflation in the dustiest place on Earth: The Bodélé Depression, Chad, *Geomorphology*, *105*, 50–58.

Chaudhry, Z., J. V. Martins, Z. Li, S.-C. Tsay, H. Chen, P. Wang, T. Wen, C. Li, and R. R. Dickerson (2007), In situ measurements of aerosol mass concentration and radiative properties in Xianghe, southeast of Beijing, *J. Geophys. Res.*, *112*, D23S90, doi:10.1029/2007JD009055.

Cheng, Y. F., et al. (2009), Influence of soot mixing state on aerosol light absorption and single scattering albedo during air mass aging at a polluted regional site in northeastern China, *J. Geophys. Res.*, *114*, D00G10, doi:10.1029/2008JD010883.

Colarco, P. R., M. R. Schoeberl, B. G. Doddridge, L. T. Marufu, O. Torres, and E. J. Welton (2004), Transport of smoke from Canadian forest fires to the surface near Washington, D.C.: Injection height, entrainment, and optical properties, *J. Geophys. Res.*, *109*, D06203, doi:10.1029/2003JD004248.

Cooke, W. F., B. Koffi, and J.-M. Gregoire (1996), Seasonality of vegetation fires in Africa from remote sensing data and application to a global chemistry model, *J. Geophys. Res.*, *101*, 21,051–21,065, doi:10.1029/96JD01835.

Derimian, Y., A. Karnieli, Y. J. Kaufman, M. O. Andreae, T. W. Andreae, O. Dubovik, W. Maenhaut, and I. Koren (2008a), The role of iron and black carbon in aerosol light absorption, *Atmos. Chem. Phys.*, *8*, 3623–3637.

Derimian, Y., J.-F. Léon, O. Dubovik, I. Chiapello, D. Tanré, A. Sinyuk, F. Auriol, T. Podvin, G. Brogniez, and B. N. Holben (2008b), Radiative properties of aerosol mixture observed during the dry season 2006 over M'Bour, Senegal (African Monsoon Multidisciplinary Analysis campaign), *J. Geophys. Res.*, *113*, D00C09, doi:10.1029/2008JD009904.

Dey, S., and S. N. Tripathi (2008), Aerosol direct radiative effects over Kanpur in the Indo-Gangetic basin, northern India: Long-term (2001–2005) observations and implications to regional climate, *J. Geophys. Res.*, *113*, D04212, doi:10.1029/2007JD009029.

Dey, S., S. N. Tripathi, and S. K. Mishra (2008), Probable mixing state of aerosols in the Indo-Gangetic Basin, northern India, *Geophys. Res. Lett.*, *35*, L03808, doi:10.1029/2007GL032622.

Dubovik, O., and M. D. King (2000), A flexible inversion algorithm for the retrieval of aerosol optical properties from Sun and sky radiance measurements, *J. Geophys. Res.*, *105*, 20,673–20,696, doi:10.1029/2000JD900282.

Dubovik, O., A. Smirnov, B. N. Holben, M. D. King, Y. J. Kaufman, T. F. Eck, and I. Slutsker (2000), Accuracy assessments of aerosol optical properties retrieved from AERONET Sun and sky-radiance measurements, *J. Geophys. Res.*, *105*, 9791–9806, doi:10.1029/2000JD900040.

Dubovik, O., B. N. Holben, T. F. Eck, A. Smirnov, Y. J. Kaufman, M. D. King, D. Tanre, and I. Slutsker (2002), Variability of absorption and optical properties of key aerosol types observed in worldwide locations, *J. Atmos. Sci.*, *59*(3), 590–608.

Dubovik, O., et al. (2006), Application of spheroid models to account for aerosol particle nonsphericity in remote sensing of desert dust, *J. Geophys. Res.*, *111*, D11208, doi:10.1029/2005JD006619.

Dwyer, E., S. Pinnock, J. M. Gregoire, and J. M. C. Pereira (2000), Global spatial and temporal distribution of vegetation fire as determined from satellite observations, *Int. J. Remote Sens.*, *21*, 1289–1302.

Eck, T. F., B. N. Holben, J. S. Reid, O. Dubovik, A. Smirnov, N. T. O'Neill, I. Slutsker, and S. Kinne (1999), Wavelength dependence of the optical depth of biomass burning, urban, and desert dust aerosols, *J. Geophys. Res.*, *104*, 31,333–31,349, doi:10.1029/1999JD900923.

Eck, T. F., B. N. Holben, D. E. Ward, O. Dubovik, J. S. Reid, A. Smirnov, M. M. Mukelabai, N. C. Hsu, N. T. O'Neill, and I. Slutsker (2001), Characterization of the optical properties of biomass burning aerosols in Zambia during the 1997 ZIBBEE Field Campaign, *J. Geophys. Res.*, *106*, 3425–3448, doi:10.1029/2000JD900555.

Eck, T. F., B. N. Holben, J. S. Reid, N. T. O'Neill, J. S. Schafer, O. Dubovik, A. Smirnov, M. A. Yamasoe, and P. Artaxo (2003), High aerosol optical depth biomass burning events: A comparison of optical properties for different source regions, *Geophys. Res. Lett.*, *30*(20), 2035, doi:10.1029/2003GL017861.

Eck, T. F., et al. (2005), Columnar aerosol optical properties at AERONET sites in central eastern Asia and aerosol transport to the tropical mid-Pacific, *J. Geophys. Res.*, *110*, D06202, doi:10.1029/2004JD005274.

Eck, T. F., et al. (2008), Spatial and temporal variability of column-integrated aerosol optical properties in the southern Arabian Gulf and United Arab Emirates in summer, *J. Geophys. Res.*, *113*, D01204, doi:10.1029/2007JD008944.

Eck, T. F., et al. (2009), Optical properties of boreal region biomass burning aerosols in central Alaska and seasonal variation of aerosol optical depth at an Arctic coastal site, *J. Geophys. Res.*, *114*, D11201, doi:10.1029/2008JD010870.

Haywood, J. M., et al. (2008), Overview of the dust and biomass-burning experiment and African monsoon multidisciplinary analysis special observing period-0, *J. Geophys. Res.*, *113*, D00C17, doi:10.1029/2008JD010077.

Holben, B. N., A. Setzer, T. F. Eck, A. Pereira, and I. Slutsker (1996), Effect of dry-season biomass burning on Amazon basin aerosol concentrations and optical properties, 1992–1994, *J. Geophys. Res.*, *101*, 19,465–19,481, doi:10.1029/96JD01114.

Holben, B. N., et al. (1998), AERONET – A federated instrument network and data archive for aerosol characterization, *Remote Sens. Environ.*, *66*, 1–16.

Holben, B. N., et al. (2001), An emerging ground-based aerosol climatology: Aerosol optical depth from AERONET, *J. Geophys. Res.*, *106*(D11), 12,067–12,097, doi:10.1029/2001JD900014.

Holben, B. N., T. F. Eck, I. Slutsker, A. Smirnov, A. Sinyuk, J. Schafer, D. Giles, and O. Dubovik (2006), AERONET's version 2.0 quality assurance criteria, Remote Sensing of Atmosphere and Clouds, *Proc. SPIE Int. Soc. Opt. Eng.*, *6408*, 64080Q, doi:10.1117/12.706524.

Hsu, N. C., S.-C. Tsay, M. D. King, and J. R. Herman (2004), Aerosol properties over bright-reflecting source regions, *IEEE Trans. Geosci. Remote Sens.*, *42*, 557–569, doi:10.1109/TGRS.2004.824067.

Huang, J., C. Zhang, and J. M. Prospero (2009), Large-scale effect of aerosols on precipitation in the West African Monsoon region, *Q. J. R. Meteorol. Soc.*, *135*, 581–594, doi:10.1002/qj.391.

Huebert, B. J., T. Bates, P. B. Russell, G. Shi, Y. J. Kim, K. Kawamura, G. Carmichael, and T. Nakajima (2003), An overview of ACE-Asia: Strategies for quantifying the relationships between Asian aerosols and their climatic impacts, *J. Geophys. Res.*, *108*(D23), 8633, doi:10.1029/2003JD003550.

Johnson, B. T., S. R. Osborne, J. M. Haywood, and M. A. J. Harrison (2008), Aircraft measurements of biomass burning aerosol over West Africa during DABEX, *J. Geophys. Res.*, *113*, D00C06, doi:10.1029/2007JD009451.

Johnson, B. T., S. Christopher, J. M. Haywood, S. R. Osborne, S. McFarlane, C. Hsu, C. Salustrod, and R. Kahn (2009), Measurements of aerosol properties from aircraft, satellite and ground-based remote sensing: A case-study from the Dust and Biomass-burning Experiment (DABEX), *Q. J. R. Meteorol. Soc.*, *135*, 922–934.

Kahn, R. A., B. J. Gaitley, J. V. Martonchik, D. J. Diner, K. A. Crean, and B. Holben (2005), Multiangle Imaging Spectroradiometer (MISR) global aerosol optical depth validation based on 2 years of coincident aerosol robotic network (AERONET) observations, *J. Geophys. Res.*, *110*, D10S04, doi:10.1029/2004JD004706.

Kotchenruther, R. A., and P. V. Hobbs (1998), Humidification factors of aerosols from biomass burning in Brazil, *J. Geophys. Res.*, *103*(D24), 32,081–32,089, doi:10.1029/98JD00340.

Lau, K. M., M. K. Kim, and K. M. Kim (2006), Asian monsoon anomalies induced by aerosol direct forcing: The role of the Tibetan Plateau, *Clim. Dyn.*, *26*, 855–864, doi:10.1007/s00382-006-0114-z.

Leahy, L. V., T. L. Anderson, T. F. Eck, and R. W. Bergstrom (2007), A synthesis of single scattering albedo of biomass burning aerosol over southern Africa during SAFARI 2000, *Geophys. Res. Lett.*, *34*, L12814, doi:10.1029/2007GL029697.

Lee, K. H., Z. Li, M. S. Wong, J. Xin, Y. Wang, W.-M. Hao, and F. Zhao (2007), Aerosol single scattering albedo estimated across China from a combination of ground and satellite measurements, *J. Geophys. Res.*, *112*, D22S15, doi:10.1029/2007JD009077.

Lewis, K., W. P. Arnott, H. Moosmüller, and C. E. Wold (2008), Strong spectral variation of biomass smoke light absorption and single scattering albedo observed with a novel dual-wavelength photoacoustic instrument, *J. Geophys. Res.*, *113*, D16203, doi:10.1029/2007JD009699.

Mallet, M., P. Tulet, D. Serça, F. Solmon, O. Dubovik, J. Pelon, V. Pont, and O. Thouron (2009), Impact of dust aerosols on the radiative budget, surface heat fluxes, heating rate profiles and convective activity over West Africa during March 2006, *Atmos. Chem. Phys.*, *9*, 7143–7160.

Martonchik, J. V., D. J. Diner, R. A. Kahn, T. P. Ackerman, M. M. Verstraete, B. Pinty, and H. R. Gordon (1998), Techniques for the retrieval of aerosol properties over land and ocean using multiangle imaging, *IEEE Trans. Geosci. Remote Sens.*, *36*, 1212–1227.

Meehl, G. A., J. M. Arblaster, and W. D. Collins (2008), Effects of black carbon aerosols on the Indian monsoon, *J. Clim.*, *21*, 2869–2882.

Menon, S., J. Hansen, L. Nazarenko, and Y. F. Luo (2002), Climate effects of black carbon aerosols in China and India, *Science*, *297*(5590), 2250–2253.

Novakov, T., M. O. Andreae, R. Gabriel, T. W. Kirchstetter, O. L. Mayol-Bracero, and V. Ramanathan (2000), Origin of carbonaceous aerosols over the tropical Indian Ocean: Biomass burning or fossil fuels?, *Geophys. Res. Lett.*, *27*, 4061–4064, doi:10.1029/2000GL011759.

O'Neill, N. T., T. F. Eck, B. N. Holben, A. Smirnov, O. Dubovik, and A. Royer (2001), Bimodal size distribution influences on the variation of Angstrom derivatives in spectral and optical depth space, *J. Geophys. Res.*, *106*, 9787–9806, doi:10.1029/2000JD900245.

O'Neill, N. T., T. F. Eck, A. Smirnov, B. N. Holben, and S. Thulasiraman (2003), Spectral discrimination of coarse and fine mode optical depth, *J. Geophys. Res.*, *108*(D17), 4559, doi:10.1029/2002JD002975.

Osborne, S. R., B. T. Johnson, J. M. Haywood, A. J. Baran, M. A. J. Harrison, and C. L. McConnell (2008), Physical and optical properties of mineral dust aerosol during the Dust and Biomass-burning Experiment, *J. Geophys. Res.*, *113*, D00C03, doi:10.1029/2007JD009551.

Prasad, A. K., R. P. Singh, and M. Kafatos (2006), Influence of coal based thermal power plants on aerosol optical properties in the Indo-Gangetic basin, *Geophys. Res. Lett.*, *33*, L05805, doi:10.1029/2005GL023801.

Prospero, J. M., P. Ginoux, O. Torres, S. E. Nicholson, and T. E. Gill (2002), Environmental characterization of global sources of atmospheric soil dust identified with the NIMBUS 7 Total Ozone Mapping Spectrometer (TOMS) absorbing aerosol product, *Rev. Geophys.*, *40*(1), 1002, doi:10.1029/2000RG000095.

Pueschel, R. F., P. B. Russell, D. A. Allen, G. V. Ferry, K. G. Snetsinger, J. M. Livingston, and S. Verma (1994), Physical and optical properties of the Pinatubo volcanic aerosol: Aircraft observations with impactors and a Sun-tracking photometer, *J. Geophys. Res.*, *99*(D6), 12,915–12,922, doi:10.1029/94JD00621.

Qin, Y., and R. M. Mitchell (2009), Characterisation of episodic aerosol types over the Australian continent, *Atmos. Chem. Phys.*, *9*, 1943–1956.

Ramanathan, V., C. Chung, D. Kim, T. Bettge, L. Buja, J. T. Kiehl, W. M. Washington, Q. Fu, D. R. Sikka, and M. Wild (2005), Atmospheric brown clouds: Impacts on South Asian climate and hydrological cycle, *Proc. Nat. Acad. Sci.*, *102*, 5326–5333.

Redemann, J., S. J. Masonis, B. Schmid, T. L. Anderson, P. B. Russell, J. M. Livingston, O. Dubovik, and A. D. Clarke (2003), Clear-column closure studies of aerosols and water vapor aboard the NCAR C-130 during ACE-Asia, 2001, *J. Geophys. Res.*, *108*(D23), 8655, doi:10.1029/2003JD003442.

Reid, J. S., T. F. Eck, S. A. Christopher, P. V. Hobbs, and B. N. Holben (1999), Use of the Angstrom exponent to estimate the variability of optical and physical properties of aging smoke particles in Brazil, *J. Geophys. Res.*, *104*, 27,473–27,489, doi:10.1029/1999JD900833.

Reid, J. S., T. F. Eck, S. A. Christopher, R. Koppmann, O. Dubovik, D. P. Eleuterio, B. N. Holben, E. A. Reid, and J. Zhang (2005), A review of biomass burning emissions part III: Intensive optical properties of biomass burning particles, *Atmos. Chem. Phys.*, *5*, 827–849.

Remer, L. A., et al. (2005), The MODIS aerosol algorithm, products, and validation, *J. Atmos. Sci.*, *62*, 947–973.

Schmid, B., J. Michalsky, R. Halthore, M. Beauharnois, L. Harrison, J. Livingston, P. Russell, B. Holben, T. Eck, and A. Smirnov (1999), Comparison of aerosol optical depth from four solar radiometers during the fall 1997 ARM intensive observation period, *Geophys. Res. Lett.*, *26*, 2725–2728, doi:10.1029/1999GL900513.

Schmid, B., et al. (2003), Column closure studies of lower tropospheric aerosol and water vapor during ACE-Asia using airborne Sun photometer and airborne in situ and ship-based lidar measurements, *J. Geophys. Res.*, *108*(D23), 8656, doi:10.1029/2002JD003361.

Singh, R. P., S. Dey, S. N. Tripathi, V. Tare, and B. Holben (2004), Variability of aerosol parameters over Kanpur, northern India, *J. Geophys. Res.*, *109*, D23206, doi:10.1029/2004JD004966.

Smirnov, A., B. N. Holben, T. F. Eck, O. Dubovik, and I. Slutsker (2000), Cloud screening and quality control algorithms for the AERONET data base, *Remote Sens. Environ.*, *73*, 337–349.

Sokolik, I. N., and O. B. Toon (1999), Incorporation of mineralogical composition into models of the radiative properties of mineral aerosol from UV to IR wavelengths, *J. Geophys. Res.*, *104*, 9423–9444.

Todd, M. C., R. Washington, J. V. Martins, O. Dubovik, G. Lizcano, S. M'Bainayel, and S. Engelstaedter (2007), Mineral dust emission from the Bodélé Depression, northern Chad, during BoDEx 2005, *J. Geophys. Res.*, *112*, D06207, doi:10.1029/2006JD007170.

Venkataraman, C., G. Habib, A. Eiguren-Fernandez, A. H. Miguel, and S. K. Friedlander (2005), Residential Biofuels in South Asia: Carbonaceous Aerosol Emissions and Climate, *Science*, *307*, 1454–1456.

Yang, M., S. G. Howell, J. Zhuang, and B. J. Huebert (2009), Attribution of aerosol light absorption to black carbon, brown carbon, and dust in China—Interpretations of atmospheric measurements during EAST-AIRE, *Atmos. Chem. Phys.*, *9*, 2035–2050.

Zhao, F., and Z. Li (2007), Estimation of aerosol single scattering albedo from solar direct spectral radiance and total broadband irradiances measured in China, *J. Geophys. Res.*, *112*, D22S03, doi:10.1029/2006JD007384.

B. Chatenet, LISA, Universités Paris-Est – Paris Diderot-Paris 7, CNRS, Créteil F- 94010, France.

H. Chen, Division for Middle Atmosphere and Remote Sensing, Chinese Academy of Sciences, Beijing 100029, China.

O. Dubovik and P. Goloub, Laboratoire d'Optique Atmospherique, Université de Lille 1, Villeneuve d'Ascq F-59655, France.

T. F. Eck, D. M. Giles, B. N. Holben, A. Sinyuk, and A. Smirnov, Biospheric Sciences Branch, NASA Goddard Space Flight Center, Greenbelt, MD 20771, USA. (thomas.f.eck@nasa.gov)

N. T. O'Neill, CARTEL, Universite de Sherbrooke, Sherbrooke, QC J1K 2R1, Canada.

R. T. Pinker and Z. Li, Department of Atmospheric and Oceanic Science, University of Maryland, College Park, MD 20742, USA.

J. S. Reid, Marine Meteorology Division, Naval Research Laboratory, Monterey, CA 93943, USA.

R. P. Singh, Computational Science and Engineering, Chapman University, Orange, CA 92866, USA.

S. N. Tripathi, Department of Civil Engineering, Indian Institute of Technology Kanpur, Kanpur 208016, India.

P. Wang and X. Xia, LAGEO, Institute of Atmospheric Physics, Chinese Academy of Sciences, Beijing 100029, China.